SRGP-1/srGAP and AFD-1/Afadin stabilize HMP-1/α-Catenin at rosettes to seal internalization sites following gastrulation in *C. elegans*

Joel M. Serre[a,], Mark M. Slabodnick[b,c], Bob Goldstein[b], and Jeff Hardin[a, d,+]

[a] Program in Genetics and [d] Department of Integrative Biology, University of Wisconsin-Madison
[b]Department of Biology, University of North Carolina at Chapel Hill, Chapel Hill, North Carolina, 27599 USA
[c]Department of Biology, Knox University, Galesburg, Illinois, 61401 USA

[+] Corresponding author:
Department of Integrative Biology, 1117 W. Johnson St., Madison, Wisconsin 53706 USA
(jdhardin@wisc.edu)

Running head: srGAP, α-catenin, and cell sealing

Keywords: gastrulation, *C. elegans*, cell-cell adhesion, cadherin/catenin complex, afadin, srGAP, rosette

Abstract

A hallmark of gastrulation is the establishment of germ layers by internalization of cells initially on the exterior. In *C. elegans* the end of gastrulation is marked by the closure of the ventral cleft, a structure formed as cells internalize during gastrulation, and the subsequent rearrangement of adjacent neuroblasts that remain on the surface. We found that a nonsense allele of *srgp-1/srGAP* leads to 10-15% cleft closure failure. Deletion of the SRGP-1 C-terminal domain led to a comparable rate of cleft closure failure, whereas deletion of the N-terminal F-BAR region resulted in milder defects. Loss of the SRGP-1 C-terminus or F-BAR domain results in defects in rosette formation and defective clustering of HMP-1/α-catenin in surface cells during cleft closure. A mutant form of HMP-1 with an open M domain can suppress cleft closure defects in *srgp-1* mutant backgrounds, suggesting that this mutation acts as a gain-of-function allele. Since SRGP-1 binding to HMP-1 is not favored in this case, we sought another HMP-1 interactor that might be recruited when HMP-1 is constitutively open. A good candidate is AFD-1/Afadin, which genetically interacts with cadherin-based adhesion later during embryonic elongation. AFD-1 is prominently expressed at the vertex of neuroblast rosettes in wildtype, and depletion of AFD-1/Afadin increases cleft closure defects in *srgp-1* and *hmp-1*$^{R551/554A}$ backgrounds. We propose that SRGP-1 promotes nascent junction formation in rosettes; as junctions mature and sustain higher levels of tension, the M domain of HMP-1 opens, allowing maturing junctions to transition from recruitment of SRGP-1 to AFD-1. Our work identifies new roles for α-catenin interactors during a process crucial to metazoan development.

Introduction

Gastrulation is a hallmark of metazoan development that establishes the basic body plan [1]. In many organisms, internalization of founder cells that form the three primary germ layers, as well as primordial germ cells, occurs via detachment of the apical surfaces of individual cells from the embryo's exterior [2-5]. Such internalization can involve an epithelial-mesenchymal transition (EMT), as cells dismantle their cell-cell junctional machinery and detach [6, 7]; in other cases, a true EMT does not occur [5, 8]. Neighboring cells that remain on the exterior must seal the breach left behind by internalizing cells, rearranging and making new cell-cell junctional connections as they do so. While cell internalization is essential for successful gastrulation in numerous organisms, most of the focus thus far has been on cellular events within internalizing cells; relatively less attention has been paid to neighboring cells that seal the embryonic exterior.

The early *C. elegans* embryo is a useful model system for understanding changes in cell-cell adhesion associated with cell internalization. Gastrulation in *C. elegans* involves stereotypical events on the ventral surface of the embryo that internalize endodermal, mesodermal, and germ cell precursors [5, 9]. The best studied of these events is the internalization of Ea and Ep, the endodermal precursors. Ea/p undergo myosin-mediated apical constriction [8, 10-13]. Germ cell precursors rely on a different mechanism, involving cadherin-dependent "hitchhiking" [14]. Concomitant with internalization of Ea/p, neighboring cells have been observed to produced protrusions that may aid resealing of the embryo's surface via active crawling [15]. Together with apical constriction of internalizing cells themselves, these movements are thought to aid cell internalization and simultaneous resealing of the ventral surface [12, 15].

A ventral cleft forms on the surface of the embryo as the last sets of cells are internalized at the end of gastrulation. The ventral cleft is surrounded by neuroblasts derived from ABplp and ABprp in the posterior and ABalp and ABarp in the anterior. The ventral gastrulation cleft is subsequently closed via movements of ventral neuroblasts toward the ventral midline between 230 and 290 minutes postfertilization, causing the ventral cleft to disappear approximately one hour before the movements of ventral epidermal enclosure begin [16, 17]. Failures in ventral cleft closure lead to highly penetrant failure of ventral enclosure (for reviews of this process, see [9, 18, 19]).

Defects in the movement of neuroblasts to close the ventral cleft are observed in embryos defective in several cell signaling pathways, including those involving Eph/ephrin signaling [16, 20, 21], PTP-3/LAR (Leukocyte Common Antigen Related Receptor, a protein tyrosine phosphatase; [22]), semaphorin-2A/MAB-20/plexin signaling [23, 24], and the *C. elegans* Kallmann syndrome ortholog *kal-1* [25, 26]. Such defects result in an enlarged or persistent ventral cleft; if the ventral cleft is not closed by the time of epidermal enclosure, enclosure movements are often disrupted.

The motile events downstream of cell signaling at the ventral cleft are poorly understood; loss of function of the SCAR/WAVE gene *wve-1* leads to significant defects in ventral neuroblast organization [27], suggesting that actin-based motility may be important for ventral neuroblast movement. Filopodial protrusions have been observed during cleft closure, but their significance is unclear [28]. As ventral neuroblasts move together, surrounding cells adjacent to the cleft must rearrange as the cleft closes [12]. After the events of ventral cleft closure, the neuroblasts that

seal the cleft divide and rearrange to form part of the presumptive ventral nerve cord before the embryo begins to elongate into a vermiform shape [9, 29]. Ventral neuroblasts later accumulate myosin foci and cadherin complex proteins [30].

Internalization of cells during gastrulation in *C. elegans* involves detachment of cells from their neighbors and establishment of new connections among cells remaining at the ventral surface, so changes in cell-cell adhesion must presumably occur during this process. The *C. elegans* cadherin/catenin complex (CCC) has been the focus of significant attention in this regard. The core components of the CCC, HMR-1/cadherin, HMP-2/β-catenin, and HMP-1/α-catenin, are present in the early embryo before gastrulation begins [11, 14, 31]. While there is not an essential requirement for cadherin-dependent adhesion during Ea/p internalization in otherwise wild-type embryos, there is a synergistic requirement for the cadherin complex when the L1CAM homologue SAX-7 or CED-5/DOCK180 is depleted [32, 33]. Accumulation of CCC components at the interface between cells that internalize and those that remain on the surface has been proposed to aid recruitment of actomyosin contractile networks necessary for internalization [5, 11], after engagement of an actomyosin-mediated "clutch" in Ea/p [13].

Much of the focus regarding the CCC during gastrulation has been on the internalizing cells, specifically Ea/p. Requirements for the CCC in subsequent internalizations have not been specifically analyzed, nor has the role of the CCC in resealing the ventral surface after internalization been assessed. We set out to investigate roles for the core CCC component, HMP-1, in these processes. In addition, we turned our attention to SRGP-1/srGAP, the lone slit/robo GTPase activating protein in *C. elegans* [28, 34]. We showed previously that SRGP-1 is a

modulator of cell-cell adhesion during the later events of ventral enclosure [28] and embryonic elongation [35, 36]. In addition, however, *srgp-1* knockdown in *hmp-1*(*fe4)* mutants leads to Gex (Gut on the exterior) phenotypes due to a failure to complete cleft closure [28], implicating it in the earlier events of internalization and ventral sealing at the end of gastrulation.

SRGP-1 is a homolog of vertebrate Slit/Robo GTPase Activating Proteins (srGAPs), which have an N-terminal F-BAR domain that associates with curved membranes, a central RhoGAP domain, and an SH3 domain which has been shown to associate with various other factors such as WAVE, WASP, and Lamellipodin [37-39]. SRGP-1 in *C. elegans* does not contain an SH3 domain; nevertheless, we showed previously that the SRGP-1 C-terminus interacts with both the N-terminal half of SRGP-1 [28] and with HMP-1 [35]. Overexpression of the F-BAR domain of SRGP-1 leads to ectopic membrane tubulations. The C-terminus of SRGP-1 is required to recruit HMP-1 into these tubulations [28] and for normal HMP-1 dynamics [36], consistent with a role for the SRGP-1 C terminus is coordinating the interaction with HMP-1.

Here we investigated the role of SRGP-1 prior to epidermal morphogenesis, as the ventral surface seals the final breaches due to cell internalization at the end of gastrulation. We found that SRGP-1 is required for normal cell behavior, cell morphology, and HMP-1 recruitment during this essential process. We also found that destabilizing salt bridge mutations within the M (middle) domain of HMP-1, which cause the M domain to remain in an extended state and abrogate binding by the SRGP-1 C terminus [35], are able to suppress SRGP-1 phenotypes. This suppression may be in part due to increased recruitment of components that interact with an open conformation of the M domain, including the *C. elegans* afadin homologue, AFD-1.

Results

Mutations in srgp-1 lead to cleft closure defects

Our prior work established a role for SRGP-1 in the embryonic epidermis in *C. elegans* [28, 35], but srGAPs in vertebrates were originally identified through their roles in the developing nervous system [39-43]. In *C. elegans*, a majority of neuroblasts are found on the ventral side of the embryo following gastrulation [9, 17]. These neuroblasts must (1) adhere to one another to keep other tissues internalized during gastrulation (reviewed in [5, 9]), (2) divide and rearrange to form part of the ventral nerve cord [29], and (3) act as a substrate for the epidermis, which undergoes epiboly during ventral enclosure [23, 30, 44]. Using 4D DIC microscopy, we observed that an appreciable percentage (11.1%) of homozygotes for *srgp-1*(*jc72*), a nonsense allele hereafter referred to as *srgp-1*^{W122Stop} (Fig. 1A), do not complete ventral cleft closure at the end of gastrulation, leading to endodermal precursors being extruded when the epidermis attempts to undergo epiboly and the contractions normally associated with embryonic elongation (Figure 1B, second row).

SRGP-1 has three major functional domains: (1) an N-terminal F-BAR domain, (2) a central GAP domain, and (3) an unstructured C-terminal region that is involved in protein-protein interactions (see Figure 1A, [28, 34, 35, 45]) We explored whether one of these domains might be important for SRGP-1 function during cleft closure. Using CRISPR/Cas9 methodology, we generated the following alleles: *srgp-1*$^{\Delta F\text{-}BAR}$, missense allele *srgp-1*^{R563A}, which prevents GAP activity [34, 46], and *srgp-1*$^{\Delta C}$, which deletes most of the region C-terminal to the GAP domain. Loss of the SRGP-1 F-BAR domain and C-terminal region both led to cleft closure defects

following gastrulation (Figure 1B). The percentages of embryos that displayed cleft closure defects were similar between *srgp-1*$^{\Delta C}$ and *srgp-1*^{W122Stop} alleles; while we observed cleft closure defects in *srgp-1*$^{\Delta F\text{-}BAR}$ mutant embryos, the lower frequency did not rise to the level of statistical significance compared to wildtype, in which we did not observe cleft closure defects (Figure 1C). As in our previous studies examining the epidermal functions of SRGP-1 [28], we did not observe any obvious defects in embryos lacking SRGP-1 GAP functionality. These results suggest that important aspects of SRGP-1 function during cleft closure are mediated through its C terminus, with the F-BAR domain playing a supporting role.

HMP-1 and SRGP-1 co-localize at the vertices of rosettes following the last internalization events of gastrulation

Gastrulation in *C. elegans* involves the internalization of progenitor cells that generate endoderm, mesoderm, and germ line tissues. As these cells move into the interior, they undergo apical constriction. As they do so, neighboring cells form transient rosettes to cover the space vacated by the departing cells [12]. We examined endogenously tagged HMP-1::mScarlet-I and SRGP-1::mNeonGreen in living embryos, beginning with ventral cleft formation through the final internalization events of gastrulation, which occur after cleft closure (Figure 2A). Two rosettes form and resolve at this stage, involving cells born on the left and right sides of the ventral cleft (Figure 2A, yellow dotted line; B, colored cells). At the vertex of the anterior rosette, where cells internalize, we observed a bright accumulation of HMP-1::mScarlet-I immediately after the internalization event (Figure 2A, white arrowhead). Subsequent to the accumulation of HMP-1 in the anterior rosette, the posterior rosette resolved and elongated along the anterior-posterior axis, forming new cell contacts as it did so (Figure 2A; yellow arrowheads

159 at 10 min indicate direction of cell movement by 20 min). Significantly, SRGP-1 also
160 accumulated at vertices in both the anterior and posterior rosettes (Fig. 2A, 0 min, arrowheads).
161
162 We previously demonstrated that homozygotes carrying a nonsense allele of *srgp-1* display
163 decreased HMP-1 junctional intensity [35]. We therefore sought to determine whether *srgp-1*
164 mutant backgrounds could influence the localization of HMP-1 during rosette formation,
165 focusing on the anterior rosette. We examined localization of HMP-1::mScarlet-I within the
166 anterior rosette before and after the final set of cell internalizations (Figure 3; blue dotted line
167 indicates internalizing cells). In a full-length, endogenously tagged *srgp-1* background, HMP-1
168 accumulated at the vertex formed by the disappearance of internalizing cells (Figure 3A, 0 min).
169 In contrast, in *srgp-1*$^{\Delta F\text{-}BAR}$ mutants HMP-1 at the vertex failed to coalesce into a single cluster
170 (Figure 3B, 0 minutes). In addition, a stable rosette no longer formed, and the remaining
171 neuroblasts instead coalesced into two rows with no central vertex (Figure 3B, yellow lines). In
172 *srgp-1*$^{\Delta C}$ mutants clusters of SRGP-1 accumulated within neuroblasts with no apparent pattern;
173 while HMP-1 was still able to coalesce around the rosette, multiple clusters with accumulated
174 HMP-1 were visible (Figure 3C). Taken together, these results indicate that both the SRGP-1 N-
175 and C-terminal regions have important roles during cleft closure. The F-BAR domain appears to
176 be important for organizing the tips of cells within rosettes into a single vertex, whereas the C-
177 terminus may play an important role in spatially organizing and interacting with HMP-1 during
178 this process.
179
180 *Destabilizing the M domain of HMP-1 suppresses cleft closure defects in* srgp-1 *mutants*

The M domain of HMP-1 forms a closed structure that is stabilized by multiple salt bridges (Figure 4A; [47]). Mutating Arginines 551 and 554 to alanines prevents two of these salt bridges from forming between MII and MIII; as a result, the HMP-1 M domain adopts a constitutively open conformation that prevents the recruitment of the SRGP-1 C-terminus [35]. Although the *hmp-1*$^{R551/554A}$ mutation abrogates interaction with the C-terminus of SRGP-1, there is evidence in vertebrates that an extended conformation of α-catenin may activate actin binding and/or recruitment of other binding partners, including vinculin [48-53] and afadin [54]. We therefore assessed whether a constitutively open conformation of HMP-1 could bypass the requirement for SRGP-1 at the end of gastrulation.

Mutants homozygous for *hmp-1*$^{R551/554A}$ and either the *srgp-1*^{W122Stop} or the *srpg-1*$^{\Delta C}$ allele displayed fewer cleft closure defects compared to *srgp-1*^{W122Stop} or *srpg-1*$^{\Delta C}$ homozygotes with wild-type *hmp-1*; in contrast, there was no change in frequency of cleft closure defects in *srgp-1*$^{\Delta F\text{-}BAR}$ homozygotes when the salt bridge mutations were introduced (Figure 4B). These results suggest that an open conformation of the HMP-1 M domain can bypass some functions normally performed by the SRGP-1 C-terminus, but that the SRGP-1 F-BAR domain is still required, presumably independently of binding of the SRGP-1 C terminus to the HMP-1 M domain.

To test if the salt bridge mutations in HMP-1 truly behave as gain-of-function mutations, we introduced these mutations into the *hmp-1*(*fe4*) background. The *hmp-1*(*fe4*) allele, hereafter referred to as *hmp-1*^{S823F}, replaces a serine with a phenylalanine (S823F) within the actin binding domain of HMP-1 and behaves as a hypomorph (Figure 4A; [55, 56]). *hmp-1*^{S823F} homozygotes display morphogenetic failure and developmental arrest at a variety of stages, including during

cleft closure. Using CRISPR/Cas9 we introduced the R551/554A mutations into the *hmp-1*^{S823F} background. Hermaphrodites homozygous for *hmp-1*$^{R551/554A;\ S823F}$ on average laid more embryos and had minimal body morphology defects compared to *hmp-1*^{S823F} homozygotes (Figure 4C,F). *hmp-1*$^{R551/554A;\ S823F}$ homozygous embryos also showed reduced lethality compared to embryos homozygous for *hmp-1*^{S823F} (Figure 4D,E). However, when we imaged *hmp-1*$^{R551/554A;\ S823F}$ embryos, we found that they were more sensitive to mechanical pressure in 10% agar mounts and required mounting on 5% agar pads (Figure S1), which we used for subsequent experiments utilizing this allele. We also observed that *hmp-1*^{S823F} homozygotes exhibited increased embryonic lethality at colder temperatures (Figure 4D). We examined whether the *hmp-1*$^{R551/554A}$ mutation suppressed *hmp-1*^{S823F} phenotypes at 15°C. The introduction of the salt bridge mutations partially suppressed embryonic lethality at 15°C, and, although it did not rise to the level of statistical significance, *hmp-1*$^{R551/554A;S823F}$ homozygotes reared at 15°C had an increase in brood size compared to *hmp-1*^{S823F} homozygotes (Figure 4C,D). Taken together, these results indicate that the *hmp-1*$^{R551/554A}$ mutation acts as a gain-of-function allele that can partially offset reduction of actin binding activity conferred by the C-terminal *S823F* mutation.

We previously utilized *hmp-1*^{S823F} hypomorphic (*hmp-1(fe4)*) homozygotes as a sensitized background to identify modulators of cadherin-dependent adhesion [57] and identified *srgp-1* as a strong enhancer of embryonic lethality in the *hmp-1*^{S823F} background. RNAi knockdown of *srgp-1* resulted in nearly total embryonic lethality, while *srgp-1* knockdown by feeding RNAi in wild-type embryos had minimal effects. At least some of the synergistic lethality was caused by Gex phenotypes during ventral enclosure [28]. We therefore examined the synergistic effect of *srgp-1* RNAi knockdown in *hmp-1*$^{R551/554A;\ S823F}$ embryos. The salt bridge mutation was able to

reduce the embryonic lethality of *srgp-1(RNAi);hmp-1*^{S823F} embryos significantly (Figure 4E). These results confirm that an open conformation of the HMP-1 M domain is able to bypass some requirements for SRGP-1, in addition to its ability to compensate for reduced actin binding activity mediated by the HMP-1 C terminus.

Loss of afd-1/afadin *function leads to increased frequency of cleft closure defects*

Conformational changes within the α-catenin M domain can affect its ability to recruit components that modulate cell adhesion. One such modulator in vertebrates is vinculin; when the αE-catenin M domain is extended, either via direct mechanical distension [58-60] or by introducing salt bridge mutations [51], its binding affinity for vinculin is increased. However, DEB-1, the vinculin homolog in *C. elegans* does not interact with HMP-1 [47], and its expression is confined to muscle cells during development [61-63], ruling it out as a candidate HMP-1 interactor that could be positively affected by the *R551/554A* salt bridge mutations in the context of cleft closure. Another candidate modulator is AFD-1/afadin. Vertebrate afadin can bind to αE-catenin [64, 65]. While there is currently no published evidence for direct binding of the *Drosophila* afadin, Canoe, to α-catenin (M. Peifer and U. Tepass, pers. commun.), Canoe localizes to cell-cell junctions and modulates morphogenesis in a variety of contexts in *Drosophila* [66-71]. Moreover, we showed previously that AFD-1 can be co-immunoprecipitated with HMP-1 [72] and that loss of *afd-1* function synergizes with the *hmp-1*^{S823F} mutation during later morphogenesis [57]. We therefore examined whether *afd-1* loss of function showed genetic interactions with *srgp-1* and with *hmp-1* salt bridge mutations.

We first determined whether *afd-1* RNAi led to cleft closure defects and lethality in wild-type embryos or in embryos homozygous for the *hmp-1*^{S823F} allele (Figure 5A-C). Knockdown of *srgp-1* or *afd-1* led to comparable levels of lethality and cleft closure defects in otherwise wild-type embryos on agar mounts. Moreover, RNAi against either *srpg-1* and *afd-1* caused a significant increase in cleft closure defects in *hmp-1*^{S823F} embryos on plates or agar mounts (Figures 5A-C). Since both *srgp-1* and *afd-1* knockdown increased the frequency of cleft closure defects in *hmp-1*^{S823F}, we examined how *afd-1* knockdown genetically interacted with *srgp-1* loss of function and with the *hmp-1*$^{R551/554A}$ mutation. In wild-type, *hmp-1*$^{R551/554A}$, and *srgp-1*^{W122Stop} backgrounds, *afd-1* knockdown resulted in an increase in cleft closure defects (Figure 5C). In *srgp-1*^{W122Stop}; *hmp-1*$^{R551/554A}$ double mutants, loss of *afd-1* resulted in a higher frequency of cleft closure defects than in *hmp-1*$^{R551/554A}$ alone, but less than in *srgp-1*^{W122Stop} mutants alone, suggesting that there may be additional factors beyond AFD-1 that may stabilize HMP-1 when it adopts an open conformation.

Computational work was previously used to engineer the actin binding domain of human αE-catenin to bind actin with higher affinity [50]. Using protein alignment, we identified the homologous amino acids in HMP-1 and generated *hmp-1*$^{QNLM676-679GSGS}$, which is predicted to bind actin with higher affinity (Figure S2A,B). Embryos homozygous for *hmp-1*$^{QNLM676-679GSGS}$ have a low level of embryonic lethality, which causes developmental arrest at various embryonic stages, including during cleft closure. These phenotypes were suppressed by loss of function of *srgp-1* and *afd-1* (Figure S2C,D). These results suggest that HMP-1 stability and linkage to the actin network must be maintained within a dynamic range during processes that contribute to cleft closure.

272

273 *AFD-1 localizes to the vertex of the anterior rosette at the end of gastrulation*

274 Since genetic perturbation of *afd-1* had consequences for cleft closure, we next assessed the
275 localization of AFD-1 during cleft closure. We visualized mKate2::AFD-1 and HMP-1::GFP
276 from cleft closure through rosette formation. While expression of mKate2::AFD-1 in the ventral
277 neuroblasts was weak, we observed strong accumulation of AFD-1 at the vertex of the anterior
278 rosette immediately following the final internalization events of gastrulation, which quickly
279 dispersed as the rosette resolved (Figure 6A). We next examined HMP-1 accumulation and
280 localization at the vertex of the anterior rosette in various mutant backgrounds (Figure 6B). Total
281 accumulation of HMP-1::GFP increased in the *hmp-1*$^{R551/554A}$ mutant background, but RNAi
282 against *afd-1* reduced total HMP-1 accumulation at the vertex, as well as the spatial extent of
283 HMP-1 accumulation at the vertex. We did not find a significant change in AFD-1 accumulation
284 in *srgp-1*^{W122Stop} mutants; while there was an increase in AFD-1 accumulation in *hmp-1*$^{R551/4A}$
285 homozygotes, it did not quite rise to statistical significance (Figure S3). These results suggest
286 that while SRGP-1 may play an important role in orienting cells during rosette formation and
287 organizing HMP-1 around the vertex, AFD-1 is essential for normal HMP-1 accumulation at the
288 vertex following the final internalization events of gastrulation. Unfortunately, we could not
289 perform the converse experiment to address whether AFD-1 recruitment requires HMP-1 at this
290 stage of development, because depletion of maternal and zygotic HMP-1 leads to catastrophic
291 morphogenetic failure, including lack of cleft closure [31, 73].

292

293 **Discussion**

294 *Rosette formation during* C. elegans *gastrulation requires cadherin-based adhesion*

Ventral cleft closure is the culmination of gastrulation in the *C. elegans* embryo. It is essential for proper organization and cohesion of neuroblasts following gastrulation, which in turn is crucial for the embryo to survive the mechanical forces that operate during later morphogenesis [5, 9, 12]. Here we have characterized the cell rearrangements that accompany sealing of the ventral surface of the embryo, as cells on the surface change position to accommodate loss of cells that internalize near the end of gastrulation. Specifically, we have demonstrated that HMP-1/α-catenin and two of its functional modulators, SRGP-1/srGAP and AFD-1/afadin, facilitate the adhesion of cells during this critical stage in embryogenesis in the *C. elegans* embryo. Based on prior work, rosettes that form as a result of earlier cell internalization events in *C. elegans* appear similar [12], so insights gleaned from studying these later events will likely be useful in understanding other internalization events in the earlier embryo.

Cell internalization is a common event during gastrulation in metazoan embryos, as cells destined for the embryo's interior detach their apical surfaces from the embryo's exterior [2-5]. Given the apical-to-basal axis of such movements during *C. elegans* gastrulation, internalization also bears similarities to other basal extrusion events, often triggered by apoptosis or cell crowding in a variety of epithelia (reviewed in [74-76]). In all these cases, however, relatively little attention has been paid to how the cells that remain on the surface seal breaches on the embryonic exterior left behind by internalizing cells. At least in some cases, such tissue sealing involves multicellular rosette formation. The geometry of these rosettes bears similarities to those associated with other morphogenetic processes, such as convergent extension [77]. An intriguing parallel to the rosettes we observed are those observed in the chick epiblast [3, 78, 79]. Although the functional significance of the rosette structures in the primitive streak is unclear,

these may reflect similar events at sites where cells depart from the surface of the embryo during gastrulation.

Rosettes in other contexts, such as during convergent extension in the *Drosophila* germband, involve modulation of adhesion complexes as cells change their connections to one another [80, 81]. In contrast, little is known about adhesive changes among neighboring non-intercalating cells that seal gaps left behind by ingressing cells. In the case of sea urchin primary mesenchyme cells, which exhibit many aspects of standard epithelial-mesenchymal transition [82], cells lose cadherin-catenin complex components at the time of ingression [82, 83]. The situation may be different in gastrulating cells in *C. elegans* and *Drosophila* neuroblasts; in the former, at least in the case of internalization of endodermal founder cells Ea and Ep, CCC components are transiently upregulated during apical constriction [11], while in the latter, post-translational loss of CCC components can be uncoupled from ingression events [84]. These differences indicate that while many processes may be conserved during internalization events, there may be a variety of mechanisms involved.

Our results shed light on this relatively understudied process by demonstrating that rosette formation at the end of gastrulation in *C. elegans* requires a robust cell-cell adhesion machinery. Reduction in the ability of HMP-1/α-catenin to bind F-actin in *hmp-1*^{S823F} mutants leads to an increase in ventral cleft closure failure, as does loss of the HMP-1 binding partner, SRGP-1. The cells surrounding the position of the vacated cell at the end of ventral cleft closure form a rosette, which ultimately resolves as cells make new connections to one another at the site of sealing.

Rosette formation is fostered by activating HMP-1/α-catenin

We and others have shown that the α-catenin M domain engages in interactions that regulate the C-terminal F-actin binding region of α-catenins [50, 85]. In this context it is striking that the *hmp-1*$^{R551/554A}$ mutation suppresses phenotypes associated with the *S823F* mutation, which we have shown previously measurably decreases the F-actin binding activity of HMP-1 [86]. Previous intragenic suppressors all clustered in the C terminus of HMP-1, not in the M domain [86]. Our present results provide further evidence that the conformation of the M domain is relevant to the ability of HMP-1 to interact, either directly or indirectly, with the actin cytoskeleton.

Rosette formation depends on proper HMP-1/a-catenin localization mediated by both the C-terminus and F-BAR domains of SRGP-1/srGAP

Salt bridges in the M domain of mammalian αE-catenin stabilize the M domain in a "closed" conformation, reducing the likelihood of association of vinculin [51, 59]. In *C. elegans*, however, we have shown previously that DEB-1/vinculin is confined to myoblasts in the early embryo, and that it does not bind HMP-1 [47, 86], suggesting that HMP-1 interacts with other effectors in non-muscle cells. In addition to its utility in identifying intramolecular interactions that regulate HMP-1 activity, the *hmp-1*^{S823F} mutation has been useful as a sensitized background for identifying such functional interactors. Both SRGP-1/srGAP and AFD-1/afadin were identified in a genome-wide RNAi screen for such interactors [57]. Our previous analysis indicated that the C terminus of SRGP-1 can physically bind the HMP-1 M domain, but, unlike the case with vertebrate aE-catenin and vinculin, not when the HMP-1 M domain is fully extended. We also

363 showed that both the N-terminal F-BAR and C-terminal domains of SRGP-1 are functionally
364 important during elongation [36].
365
366 Our analysis here also revealed roles for the N- and C-terminal regions of SRGP-1 during ventral
367 cleft closure. HMP-1 becomes highly concentrated at the tips of cells at rosette vertices in
368 embryos expressing endogenously tagged, full-length SRGP-1. The greater severity of gross
369 morphological defects in *srgp-1* nonsense and C-terminal deletion mutants further suggests a
370 more stringent requirement for the C terminus, which is lacking in both mutants, in stabilizing
371 HMP-1. Since the SRGP-1 C terminus is intact in *srgp-1*$^{\Delta F\text{-}BAR}$ mutants, it is possible that,
372 whereas SRGP-1$^{\Delta F\text{-}BAR}$ can no longer interact with the membrane directly to stabilize the CCC,
373 when the N-terminus is absent SRGP-1 can still interact with HMP-1 in some functional
374 capacity. In this case HMP-1 presumably exclusively relies on its association with the HMP-
375 1/HMP-2/HMR-1 heterotrimeric complex to associate with the plasma membrane, which is less
376 efficient in recruiting HMP-1 at sites of high membrane curvature, such as cell tips at rosette
377 vertices. The likelihood of this possibility is strengthened by our observation that *srgp-1*$^{\Delta F\text{-}BAR}$
378 homozygous embryos exhibit less lethality than *srgp-1*^{W122Stop} and *srgp-1*$^{\Delta C}$ homozygotes. In our
379 previous work we suggested that there may be a second region of SRGP-1, which lies N-terminal
380 to the C-terminal region, that can interact with some junctional component— possibly including
381 HMP-1 [28, 36]; our present work is consistent with this possibility.
382
383 A distinct role for the SRGP-1 N terminus is also suggested by our results. When the SRGP-1 F-
384 BAR domain is deleted the tips of cells in the rosette are blunted and HMP-1 forms multiple
385 aggregates in cells in the rosette, leading to less robust rosettes. In our previous work we

observed reduced membrane curvature at the leading edge during ventral epidermal enclosure, suggesting that SRGP-1 promotes highly curved membranes [28]. Our present results are consistent with a similar role at nascent rosette vertices, which require that the plasma membranes of cell tips in the rosette adopt a high degree of curvature. SRGP-1 may either stabilize such highly curved regions of the plasma membrane or be recruited to such sites, leading to clustering of HMP-1 at such sites to stabilize nascent adhesions. The loss of normal HMP-1 accumulation at cell tips in *hmp-1*$^{\Delta F\text{-}BAR}$ mutants is consistent with this possibility and suggests that not only is membrane curvature adversely affected, but that HMP-1 recruitment to sites of high membrane curvature is reduced, with adverse effects on rosettes.

The *hmp-1*$^{R551/554A}$ mutation, which maintains the HMP-1 M domain in an open conformation [36], can suppress cleft closure defects caused by loss of the SRGP-1 C-terminus, but not those resulting from loss of the SRGP-1 F-BAR domain (see Figure 4B). There are several potential explanations for this result. One possibility is that the C terminus of SRGP-1 regulates HMP-1 function beyond localization. For example, the C terminus of SRGP-1, once bound, could facilitate further opening and activation of the HMP-1 M domain, leading to recruitment of other binding partners. Constitutive opening of the HMP-1 M domain in *hmp-1*$^{R551/554A}$ mutants could obviate this requirement. Alternatively, if the major role of the SRGP-1 C terminus is to fine-tune the localization or stability of HMP-1, the enhanced activity of a fully open HMP-1 could offset the quantitative loss of HMP-1 at nascent junctions in rosettes.

Rosette formation is fostered by recruitment of AFD-1/afadin

AFD-1 accumulation at the vertex of the anterior rosette is striking compared to the low levels of AFD-1 accumulation elsewhere at this stage of development, including the posterior rosette, within which we did not see a similar accumulation of AFD-1. This indicates that junctions at the anterior rosette vertex are unique among cell-cell adhesions between ventral cells in the embryo at this stage, and that AFD-1/afadin is crucial for stabilizing them. Vertebrate afadin and *Drosophila* Canoe are recruited to junctions under increased tension or to sites with increased cellular (and hence actomyosin) dynamics [87-89]. In *C. elegans*, during later development when the epidermis is under substantial mechanical tension, AFD-1 appears at epidermal cell-cell junctions [57], consistent with tension-induced recruitment at that stage. That AFD-1 is recruited to the tips of cells in the anterior rosette vertex at the end of gastrulation suggests that the tips of these cells likewise experience increased tension. As the internalization event that forms the anterior rosette concludes, multiple cells must converge to create new contact points, which are susceptible to mechanical failure. A similar accumulation of AFD-1 is not observed in the posterior rosette, however. Notably, the cells of the posterior rosette undergo rapid extension shortly after rosette formation, whereas the anterior rosette persists. Work in *Drosophila* has demonstrated a necessity for Canoe localization to maintain tricellular junctions experiencing high tension; however, prolonged and continued accumulation of Canoe at junctions prevents vertex resolution during cell rearrangement [90]. If AFD-1 works in a similar fashion in *C. elegans*, this could imply that AFD-1 is required to stabilize the anterior rosette under higher mechanical loads.

We also found that, as is the case for *srgp-1,* loss of *afd-1* function leads to ventral cleft closure defects that can be suppressed via the *hmp-1*$^{R551/554A}$ mutation. Moreover, simultaneous depletion

of SRGP-1 and AFD-1 leads to synergistic ventral cleft closure defects. One reasonable model that accounts for this data is that, while SRGP-1 fosters the initial recruitment of HMP-1 to nascent contact sites within rosettes, AFD-1 subsequently stabilizes more mature adhesions, allowing them to withstand tension prior to rosette resolution. In this case, forcing HMP-1 into an open conformation may be able to bypass functional requirements for SRGP-1 by increasing the stability of adhesions through additional AFD-1 recruitment. It remains unclear whether AFD-1 can directly interact with HMP-1 in the way that their vertebrate counterparts do [54, 65], or if AFD-1 is recruited to cell-cell adhesion sites through other effectors that in turn depend on an open conformation of HMP-1. Since defects in *afd-1*(RNAi); *srpg-1*^{W122Stop} double loss-of-function embryos are still suppressed by *hmp-1*$^{R551/554A}$, there may be additional mechanisms that are stimulated by an open conformation of the HMP-1 M domain.

In conclusion, this work has clarified how cadherin-dependent adhesion between non-internalizing neighbors of internalizing cells, supported by SRGP-1/srGAP and AFD-1/afadin, stabilizes nascent cell-cell adhesions following the internalization events of gastrulation. Future work focused on identifying other factors that play a role in anterior rosette formation and that dissects the mechanisms through which SRGP-1, AFD-1, and HMP-1 work together in this process should continue to clarify the cellular events of tissue sealing following internalization.

Acknowledgements

Some strains were provided by the *C. elegans* Genetics Center, which is funded by the NIH Office of Research Infrastructure Programs (P40 OD010440). JS and JH were supported by NIH

453 grants R01GM058038, R01GM127687, and R35GM145312. BG was supported by NIH grant
454 R35GM134838. MMS was supported by NIH grant F32GM119348

455

456 **Contributions**

457 JMS designed, implemented, and analyzed experiments, designed and generated the novel *srgp-1*
458 and *hmp-1* CRISPR alleles, and wrote and edited drafts of the manuscript. MMS generated the
459 *afd-1* knock-in allele. BG commented on the manuscript. JH oversaw experimental design,
460 implementation, and analysis and edited the manuscript.

461

462 **Figure Legends**

463 **Figure 1 Genetic perturbation of *srgp-1* leads to cleft closure defects. (A)** A map depicting
464 the domains of SRGP-1 including mutants used in this study (*srgp-1*^{W122Stop}, *srgp-1*^{R563A}, *srgp-*
465 *1*$^{\Delta F\text{-}BAR}$, and *srgp-1*$^{\Delta C}$). **(B)** DIC images of embryos over 230 minutes. White dotted lines depict
466 the ventral cleft. The first row depicts a typical wild-type embryo proceeding through cleft
467 closure and into early elongation. *srgp-1*^{W122Stop}, *srgp-1*$^{\Delta F\text{-}BAR}$, and *srgp-1*$^{\Delta C}$ mutants all display
468 cleft closure failure, resulting in extruded endoderm (yellow dotted lines). Scale bar is 10 μm.
469 (C) A graph depicting percentage cleft closure defects in wild-type and *srgp-1* mutants. ****, p
470 < 0.0001; *, p < 0.05.

471 **Figure 2 Rosette formation leads to cell rearrangement during cleft closure. (A)** An embryo
472 expressing SRGP-1::mNeonGreen and HMP-1::mScarlet-I before, during, and after anterior
473 rosette formation (ventral view), showing the cell rearrangements that take place to seal the
474 ventral cleft. Times are relative to formation of the anterior rosette (t = 0 min). White dotted lines
475 outline cells involved in rosette formation. Blue dotted lines indicate cells that internalize. White

476 arrowhead indicates the vertex of the anterior rosette. Yellow arrows indicate the direction of cell
477 movement at the posterior end of the embryo following anterior rosette formation. **(B)** Cell
478 tracings of the embryos in (A). Internalizing cells are colored grey, cells that form rosettes are
479 colored, all other cells are white. Scale bar is 10 µm.

480 **Figure 3 *srgp-1* mutants display aberrant HMP-1::mScarlet-I aggregation and anterior**
481 **rosette formation.** Representative embryos expressing full-length or deleted SRGP-
482 1::mNeonGreen, as well as HMP-1::mScarlet-I. (**A**) SRGP-1::mNeonGreen**;** (**B**) SRGP-$1^{\Delta F\text{-}BAR}$::mNeonGreen; **(C)** SRGP-$1^{\Delta C}$::mNeonGreen. Blue dotted lines indicate cell internalization
484 that precedes formation of rosettes. White arrowheads indicate the vertex of the rosette following
485 cell internalization. White dotted lines outline cells that contribute to the rosette; yellow dotted
486 lines depict cells arranged around the vertex of the rosette. Scale bar is 5 µm.

487 **Figure 4 The *hmp-*$1^{R551/554A}$ mutation suppresses defects due to *srgp-1* loss of function and**
488 **reduced actin binding ability of HMP-1. (A)** A domain map of HMP-1 depicting the sites of
489 the R551/554A and S823F variations. **(B)** Percentage cleft closure defects in *srgp-1* and *hmp-*
490 $1^{R551/554A}$ mutants. **(C)** Fecundity of wildtype and various *hmp-1* mutants at 20°C and 15°C. **(D)**
491 Embryonic lethality of wildtype and various *hmp-1* mutants at 20°C and 15°C. **(E)** Embryonic
492 lethality of wildtype and various *hmp-1* mutants subjected to control (empty vector L4440) or
493 *srgp-1* RNAi. **(F)** *hmp-*1^{S823F} and *hmp-*$1^{R551/554A;\ S823F}$ hermaphrodites. Yellow arrowheads
494 indicate abnormally shaped or swollen regions along the body. Red dotted lines indicate clubbed
495 tails. Scale bar is 200 µm. ****, $p < 0.0001$; ***, $p<0.001$; **, $p<0.01$; *, $p < 0.05$.

496 **Figure 5 *srgp-1* and *hmp-1* genetically interact with *afd-1* during cleft closure. (A)** DIC
497 images of *hmp-*1^{S823F}, *hmp-*1^{S823F}*; srgp-1(RNAi)*, and *hmp-*1^{S823F}*; afd-1(RNAi)* embryos over the

course of 270 minutes. Dotted white lines outline the ventral cleft. Yellow dotted lines indicate extruded gut. Scale bar is 10 µm. **(B)** A stacked bar plot indicating the percentage of embryos that die during cleft closure, head enclosure, and elongation in various genetic backgrounds. *afd-1* and *srgp-1* knockdown in the *hmp-1*^{S823F} background both significantly increase the percentage of cleft closure defects. **(C)** Percent cleft closure defects in various genetic backgrounds with or without depletion of *srgp-1* and *afd-1* via RNAi. **(D)** Percentage of cleft closure defects in embryos treated with Control or *afd-1* RNAi. ****, $p < 0.0001$; ***, $p<0.001$; *, $p < 0.05$.

Figure 6 AFD-1 accumulates at the vertex of the anterior rosette. (A) A typical embryo expressing HMP-1::GFP and mKate2::AFD-1 before, during, and after anterior rosette formation. White dotted line outlines cells that form the rosette. Blue dotted lines mark the anterior cells that internalize prior to formation of the rosette. White arrowheads indicate the vertex of the rosette. Scale bar is 10 µm. **(B)** Images of HMP-1::GFP and mKate2::AFD-1 localization at the anterior rosette immediately following internalization in various genetic backgrounds. White dotted lines outline cells forming the rosette; yellow dotted lines indicate ventral cleft that remains open. Scale bar is 5 µm. **(C)** A graph depicting the total accumulation of HMP-1::GFP at the anterior rosette. (D) Graph depicting the area of HMP-1::GFP aggregation at the vertex of the anterior rosette. ****, $p < 0.0001$; ***, $p<0.001$; **, $p<0.01$; *, $p < 0.05$.

Figure 7. Summary of the roles of SRGP-1 and AFD-1 in stabilizing HMP-1 at rosettes. (A) A protein map depicting the proposed functional roles of SRGP-1 domains. **(B)** Visual summary of HMP-1 and SRGP-1 distribution in cells in different *srgp-1* mutant backgrounds. **(C)** Genetic pathways summarizing proposed routes by which HMP-1 is stabilized in wild-type and *srgp-1*^{W122Stop}; *hmp-1*$^{R551/554A}$ backgrounds

Materials and Methods

Strains and genetics

C. elegans were maintained using standard methods. Bristol N2 was used as wildtype. A complete list of strains and genotypes used in this manuscript can be found in Supplementary Table 1.

DIC imaging

Four dimensional DIC movies were collected on either a Nikon Optiphot-2 microscope connected to a QiCAM camera (QImaging) or an Olympus BX50 microscope connected to a Scion CFW-1512M camera (Scion Corp.) using Micro-Manager software (v. 1.42) [91, 92]. ImageJ plugins (https://worms.zoology.wisc.edu/research/4d/4d.html) were used to compress and view DIC movies. All embryos were mounted on 10% agar pads in M9 solution unless otherwise specified.

Confocal imaging

Embryos were dissected from adult hermaphrodites and mounted onto 10% agar pads in M9 solution and imaged. For fluorescence imaging, a Dragonfly 500 spinning disc confocal microscope (Andor Corp.), mounted on a Leica DMi8 microscope, equipped with an iXon-EMCCD camera and controlled by Fusion software (Andor Corp.) was used to collect images using 0.21 μm slices with a 63×/1.3 NA glycerol Leica objective at 20°C.

CRISPR/Cas9 genome editing

All novel knock-in and deletion alleles with *jc##* designation were generated via plasmid-based CRISPR/Cas9 [93] using repair templates cloned by SapTrap cloning [94]. Small substitution mutations were made via marker-free genome editing [95]. Guides, homology arm primers, and single-stranded repair templates for all CRISPR/Cas9 editing can be found in Supplementary Table 2.

Injection RNAi

Injection RNAi was performed by synthesizing double-stranded RNA (dsRNA) using a T7 Megascript kit (Invitrogen). The templates for *srgp-1* and control RNAi were obtained from a feeding library [96]. pIC386 was used as a template for production of *afd-1* dsRNA. dsRNA was injected at a concentration of 2µg/µL in nuclease free water. L4 worms were injected and aged overnight before embryos were dissected from mature adults for imaging.

Quantification and analysis

Percentage cleft closure defects were measured from embryos mounted for DIC imaging. Embryonic lethality was quantified by dividing the number of unhatched embryos laid on a plate by the total number of embryos on the plate from a single hermaphrodite. Total accumulation (integrated signal) and aggregation size for HMP-1::GFP were measured by drawing a circle around GFP signal at the vertex immediately following the internalization event.

Statistical analysis

566 Data from control and experimental groups were compared using one-way ANOVA with Tukey
567 post hoc testing to assess significance between individual groups. All statistical analyses were
568 carried out in Prism (GraphPad Corp.).
569

References

1. Solnica-Krezel L, Sepich DS. Gastrulation: making and shaping germ layers. Annu Rev Cell Dev Biol. 2012;28:687-717. Epub 20120709. doi: 10.1146/annurev-cellbio-092910-154043. PubMed PMID: 22804578.
2. Byrum CA. An analysis of hydrozoan gastrulation by unipolar ingression. Dev Biol. 2001;240(2):627-40. doi: 10.1006/dbio.2001.0484. PubMed PMID: 11784088.
3. Wagstaff LJ, Bellett G, Mogensen MM, Munsterberg A. Multicellular rosette formation during cell ingression in the avian primitive streak. Dev Dyn. 2008;237(1):91-6. doi: 10.1002/dvdy.21390. PubMed PMID: 18069691.
4. Shook DR, Keller R. Epithelial type, ingression, blastopore architecture and the evolution of chordate mesoderm morphogenesis. J Exp Zool B Mol Dev Evol. 2008;310(1):85-110. doi: 10.1002/jez.b.21198. PubMed PMID: 18041055.
5. Goldstein B, Nance J. Caenorhabditis elegans Gastrulation: A Model for Understanding How Cells Polarize, Change Shape, and Journey Toward the Center of an Embryo. Genetics. 2020;214(2):265-77. doi: 10.1534/genetics.119.300240. PubMed PMID: 32029580; PubMed Central PMCID: PMCPMC7017025.
6. Mareel M, Bracke M, Van Roy F, Vakaet L. Expression of E-cadherin in embryogenetic ingression and cancer invasion. Int J Dev Biol. 1993;37(1):227-35. PubMed PMID: 8507565.
7. Wu SY, Ferkowicz M, McClay DR. Ingression of primary mesenchyme cells of the sea urchin embryo: a precisely timed epithelial mesenchymal transition. Birth Defects Res C Embryo Today. 2007;81(4):241-52. doi: 10.1002/bdrc.20113. PubMed PMID: 18228256.
8. Harrell JR, Goldstein B. Internalization of multiple cells during C. elegans gastrulation depends on common cytoskeletal mechanisms but different cell polarity and cell fate regulators. Dev Biol. 2011;350(1):1-12. Epub 20100926. doi: 10.1016/j.ydbio.2010.09.012. PubMed PMID: 20875815; PubMed Central PMCID: PMCPMC3022094.
9. Chisholm AD, Hardin J. Epidermal morphogenesis. WormBook. 2005:1-22. Epub 20051201. doi: 10.1895/wormbook.1.35.1. PubMed PMID: 18050408; PubMed Central PMCID: PMCPMC4781537.
10. Lee JY, Marston DJ, Walston T, Hardin J, Halberstadt A, Goldstein B. Wnt/Frizzled signaling controls C. elegans gastrulation by activating actomyosin contractility. Curr Biol. 2006;16(20):1986-97. doi: 10.1016/j.cub.2006.08.090. PubMed PMID: 17055977; PubMed Central PMCID: PMCPMC2989422.
11. Marston DJ, Higgins CD, Peters KA, Cupp TD, Dickinson DJ, Pani AM, et al. MRCK-1 Drives Apical Constriction in C. elegans by Linking Developmental Patterning to Force Generation. Curr Biol. 2016;26(16):2079-89. Epub 20160721. doi: 10.1016/j.cub.2016.06.010. PubMed PMID: 27451898; PubMed Central PMCID: PMCPMC4996705.
12. Pohl C, Tiongson M, Moore JL, Santella A, Bao Z. Actomyosin-based self-organization of cell internalization during C. elegans gastrulation. BMC Biol. 2012;10:94. Epub 20121130. doi: 10.1186/1741-7007-10-94. PubMed PMID: 23198792; PubMed Central PMCID: PMCPMC3583717.
13. Roh-Johnson M, Shemer G, Higgins CD, McClellan JH, Werts AD, Tulu US, et al. Triggering a cell shape change by exploiting preexisting actomyosin contractions. Science. 2012;335(6073):1232-5. Epub 20120209. doi: 10.1126/science.1217869. PubMed PMID: 22323741; PubMed Central PMCID: PMCPMC3298882.

14. Chihara D, Nance J. An E-cadherin-mediated hitchhiking mechanism for C. elegans germ cell internalization during gastrulation. Development. 2012;139(14):2547-56. Epub 20120606. doi: 10.1242/dev.079863. PubMed PMID: 22675206; PubMed Central PMCID: PMCPMC3383229.
15. Nance J, Priess JR. Cell polarity and gastrulation in C. elegans. Development. 2002;129(2):387-97. doi: 10.1242/dev.129.2.387. PubMed PMID: 11807031.
16. George SE, Simokat K, Hardin J, Chisholm AD. The VAB-1 Eph receptor tyrosine kinase functions in neural and epithelial morphogenesis in C. elegans. Cell. 1998;92(5):633-43. doi: 10.1016/s0092-8674(00)81131-9. PubMed PMID: 9506518.
17. Sulston JE, Schierenberg E, White JG, Thomson JN. The embryonic cell lineage of the nematode Caenorhabditis elegans. Developmental Biology. 1983;100(1):64-119. doi: 10.1016/0012-1606(83)90201-4.
18. Carvalho CA, Broday L. Game of Tissues: How the Epidermis Thrones C. elegans Shape. J Dev Biol. 2020;8(1). Epub 20200309. doi: 10.3390/jdb8010007. PubMed PMID: 32182901; PubMed Central PMCID: PMCPMC7151205.
19. Vuong-Brender TT, Yang X, Labouesse M. C. elegans Embryonic Morphogenesis. Curr Top Dev Biol. 2016;116:597-616. Epub 20160201. doi: 10.1016/bs.ctdb.2015.11.012. PubMed PMID: 26970644.
20. Chin-Sang ID, George SE, Ding M, Moseley SL, Lynch AS, Chisholm AD. The ephrin VAB-2/EFN-1 functions in neuronal signaling to regulate epidermal morphogenesis in C. elegans. Cell. 1999;99(7):781-90. doi: 10.1016/s0092-8674(00)81675-x. PubMed PMID: 10619431.
21. Chin-Sang ID, Moseley SL, Ding M, Harrington RJ, George SE, Chisholm AD. The divergent C. elegans ephrin EFN-4 functions inembryonic morphogenesis in a pathway independent of the VAB-1 Eph receptor. Development. 2002;129(23):5499-510. doi: 10.1242/dev.00122. PubMed PMID: 12403719.
22. Harrington RJ, Gutch MJ, Hengartner MO, Tonks NK, Chisholm AD. The C. elegans LAR-like receptor tyrosine phosphatase PTP-3 and the VAB-1 Eph receptor tyrosine kinase have partly redundant functions in morphogenesis. Development. 2002;129(9):2141-53. doi: 10.1242/dev.129.9.2141. PubMed PMID: 11959824.
23. Ikegami R, Simokat K, Zheng H, Brown L, Garriga G, Hardin J, et al. Semaphorin and Eph receptor signaling guide a series of cell movements for ventral enclosure in C. elegans. Curr Biol. 2012;22(1):1-11. Epub 20111222. doi: 10.1016/j.cub.2011.12.009. PubMed PMID: 22197242; PubMed Central PMCID: PMCPMC4306670.
24. Nakao F, Hudson ML, Suzuki M, Peckler Z, Kurokawa R, Liu Z, et al. The PLEXIN PLX-2 and the ephrin EFN-4 have distinct roles in MAB-20/Semaphorin 2A signaling in Caenorhabditis elegans morphogenesis. Genetics. 2007;176(3):1591-607. Epub 20070516. doi: 10.1534/genetics.106.067116. PubMed PMID: 17507686; PubMed Central PMCID: PMCPMC1931547.
25. Hudson ML, Kinnunen T, Cinar HN, Chisholm AD. C. elegans Kallmann syndrome protein KAL-1 interacts with syndecan and glypican to regulate neuronal cell migrations. Dev Biol. 2006;294(2):352-65. Epub 20060503. doi: 10.1016/j.ydbio.2006.02.036. PubMed PMID: 16677626.
26. Rugarli EI, Di Schiavi E, Hilliard MA, Arbucci S, Ghezzi C, Facciolli A, et al. The Kallmann syndrome gene homolog in C. elegans is involved in epidermal morphogenesis and

neurite branching. Development. 2002;129(5):1283-94. doi: 10.1242/dev.129.5.1283. PubMed PMID: 11874923.

27. Withee J, Galligan B, Hawkins N, Garriga G. Caenorhabditis elegans WASP and Ena/VASP proteins play compensatory roles in morphogenesis and neuronal cell migration. Genetics. 2004;167(3):1165-76. doi: 10.1534/genetics.103.025676. PubMed PMID: 15280232; PubMed Central PMCID: PMCPMC1470955.

28. Zaidel-Bar R, Joyce MJ, Lynch AM, Witte K, Audhya A, Hardin J. The F-BAR domain of SRGP-1 facilitates cell-cell adhesion during C. elegans morphogenesis. J Cell Biol. 2010;191(4):761-9. Epub 20101108. doi: 10.1083/jcb.201005082. PubMed PMID: 21059849; PubMed Central PMCID: PMCPMC2983056.

29. Shah PK, Tanner MR, Kovacevic I, Rankin A, Marshall TE, Noblett N, et al. PCP and SAX-3/Robo Pathways Cooperate to Regulate Convergent Extension-Based Nerve Cord Assembly in C. elegans. Dev Cell. 2017;41(2):195-203 e3. doi: 10.1016/j.devcel.2017.03.024. PubMed PMID: 28441532; PubMed Central PMCID: PMCPMC5469364.

30. Wernike D, Chen Y, Mastronardi K, Makil N, Piekny A. Mechanical forces drive neuroblast morphogenesis and are required for epidermal closure. Dev Biol. 2016;412(2):261-77. Epub 20160227. doi: 10.1016/j.ydbio.2016.02.023. PubMed PMID: 26923492.

31. Costa M, Raich W, Agbunag C, Leung B, Hardin J, Priess JR. A putative catenin-cadherin system mediates morphogenesis of the Caenorhabditis elegans embryo. J Cell Biol. 1998;141(1):297-308. doi: 10.1083/jcb.141.1.297. PubMed PMID: 9531567; PubMed Central PMCID: PMCPMC2132712.

32. Grana TM, Cox EA, Lynch AM, Hardin J. SAX-7/L1CAM and HMR-1/cadherin function redundantly in blastomere compaction and non-muscle myosin accumulation during Caenorhabditis elegans gastrulation. Dev Biol. 2010;344(2):731-44. Epub 20100531. doi: 10.1016/j.ydbio.2010.05.507. PubMed PMID: 20515680; PubMed Central PMCID: PMCPMC2914123.

33. Sawyer JM, Glass S, Li T, Shemer G, White ND, Starostina NG, et al. Overcoming redundancy: an RNAi enhancer screen for morphogenesis genes in Caenorhabditis elegans. Genetics. 2011;188(3):549-64. Epub 20110428. doi: 10.1534/genetics.111.129486. PubMed PMID: 21527776; PubMed Central PMCID: PMCPMC3176534.

34. Neukomm LJ, Frei AP, Cabello J, Kinchen JM, Zaidel-Bar R, Ma Z, et al. Loss of the RhoGAP SRGP-1 promotes the clearance of dead and injured cells in Caenorhabditis elegans. Nat Cell Biol. 2011;13(1):79-86. Epub 20101219. doi: 10.1038/ncb2138. PubMed PMID: 21170032; PubMed Central PMCID: PMCPMC3808961.

35. Serre JM, Lucas B, Martin SCT, Heier JA, Shao X, Hardin J. A C. elegans srGAP is a novel α-catenin M domain-binding protein that strengthens cadherin-dependent adhesion during morphogenesis. Development. in revision.

36. Serre JM, Lucas B, Martin SCT, Heier JA, Shao X, Hardin J. C. elegans srGAP is an alpha-catenin M domain-binding protein that strengthens cadherin-dependent adhesion during morphogenesis. Development. 2022;149(18). Epub 20220920. doi: 10.1242/dev.200775. PubMed PMID: 36125129.

37. Guerrier S, Coutinho-Budd J, Sassa T, Gresset A, Jordan NV, Chen K, et al. The F-BAR domain of srGAP2 induces membrane protrusions required for neuronal migration and morphogenesis. Cell. 2009;138(5):990-1004. doi: 10.1016/j.cell.2009.06.047. PubMed PMID: 19737524; PubMed Central PMCID: PMCPMC2797480.

38. Endris V, Haussmann L, Buss E, Bacon C, Bartsch D, Rappold G. SrGAP3 interacts with lamellipodin at the cell membrane and regulates Rac-dependent cellular protrusions. J Cell Sci. 2011;124(Pt 23):3941-55. Epub 20111208. doi: 10.1242/jcs.077081. PubMed PMID: 22159416.
39. Lucas B, Hardin J. Mind the (sr)GAP - roles of Slit-Robo GAPs in neurons, brains and beyond. J Cell Sci. 2017;130(23):3965-74. Epub 20171102. doi: 10.1242/jcs.207456. PubMed PMID: 29097383; PubMed Central PMCID: PMCPMC5769592.
40. Endris V, Wogatzky B, Leimer U, Bartsch D, Zatyka M, Latif F, et al. The novel Rho-GTPase activating gene MEGAP/ srGAP3 has a putative role in severe mental retardation. Proc Natl Acad Sci U S A. 2002;99(18):11754-9. Epub 20020823. doi: 10.1073/pnas.162241099. PubMed PMID: 12195014; PubMed Central PMCID: PMCPMC129341.
41. Wong K, Ren X-R, Huang Y-Z, Xie Y, Liu G, Saito H, et al. Signal Transduction in Neuronal Migration. Cell. 2001;107(2):209-21. doi: 10.1016/s0092-8674(01)00530-x.
42. Foletta VC, Brown FD, Scott Young Iii W. Cloning of rat ARHGAP4/C1, a RhoGAP family member expressed in the nervous system that colocalizes with the Golgi complex and microtubules. Molecular Brain Research. 2002;107(1):65-79. doi: 10.1016/s0169-328x(02)00448-5.
43. Katoh M, Katoh M. Identification and characterization of human FCHSD1 and FCHSD2 genes in silico. International Journal of Molecular Medicine. 2004. doi: 10.3892/ijmm.13.5.749.
44. Fotopoulos N, Wernike D, Chen Y, Makil N, Marte A, Piekny A. Caenorhabditis elegans anillin (ani-1) regulates neuroblast cytokinesis and epidermal morphogenesis during embryonic development. Dev Biol. 2013;383(1):61-74. Epub 20130907. doi: 10.1016/j.ydbio.2013.08.024. PubMed PMID: 24016757.
45. Neukomm LJ, Zeng S, Frei AP, Huegli PA, Hengartner MO. Small GTPase CDC-42 promotes apoptotic cell corpse clearance in response to PAT-2 and CED-1 in C. elegans. Cell Death Differ. 2014;21(6):845-53. Epub 20140314. doi: 10.1038/cdd.2014.23. PubMed PMID: 24632947; PubMed Central PMCID: PMCPMC4013519.
46. Barrett T, Xiao B, Dodson EJ, Dodson G, Ludbrook SB, Nurmahomed K, et al. The structure of the GTPase-activating domain from p50rhoGAP. Nature. 1997;385(6615):458-61. doi: 10.1038/385458a0. PubMed PMID: 9009196.
47. Kang H, Bang I, Jin KS, Lee B, Lee J, Shao X, et al. Structural and functional characterization of Caenorhabditis elegans alpha-catenin reveals constitutive binding to beta-catenin and F-actin. J Biol Chem. 2017;292(17):7077-86. Epub 20170315. doi: 10.1074/jbc.M116.769778. PubMed PMID: 28298447; PubMed Central PMCID: PMCPMC5409474.
48. Pang SM, Le S, Kwiatkowski AV, Yan J. Mechanical stability of alphaT-catenin and its activation by force for vinculin binding. Mol Biol Cell. 2019;30(16):1930-7. Epub 20190718. doi: 10.1091/mbc.E19-02-0102. PubMed PMID: 31318313; PubMed Central PMCID: PMCPMC6727763.
49. Seddiki R, Narayana G, Strale PO, Balcioglu HE, Peyret G, Yao M, et al. Force-dependent binding of vinculin to alpha-catenin regulates cell-cell contact stability and collective cell behavior. Mol Biol Cell. 2018;29(4):380-8. Epub 20171227. doi: 10.1091/mbc.E17-04-0231. PubMed PMID: 29282282; PubMed Central PMCID: PMCPMC6014167.
50. Ishiyama N, Sarpal R, Wood MN, Barrick SK, Nishikawa T, Hayashi H, et al. Force-dependent allostery of the alpha-catenin actin-binding domain controls adherens junction dynamics and functions. Nat Commun. 2018;9(1):5121. Epub 20181130. doi: 10.1038/s41467-018-07481-7. PubMed PMID: 30504777; PubMed Central PMCID: PMCPMC6269467.

751 51. Barrick S, Li J, Kong X, Ray A, Tajkhorshid E, Leckband D. Salt bridges gate alpha-
752 catenin activation at intercellular junctions. Mol Biol Cell. 2018;29(2):111-22. Epub 20171115.
753 doi: 10.1091/mbc.E17-03-0168. PubMed PMID: 29142072; PubMed Central PMCID:
754 PMCPMC5909925.
755 52. Yao M, Qiu W, Liu R, Efremov AK, Cong P, Seddiki R, et al. Force-dependent
756 conformational switch of alpha-catenin controls vinculin binding. Nat Commun. 2014;5:4525.
757 Epub 20140731. doi: 10.1038/ncomms5525. PubMed PMID: 25077739.
758 53. Yonemura S, Wada Y, Watanabe T, Nagafuchi A, Shibata M. alpha-Catenin as a tension
759 transducer that induces adherens junction development. Nat Cell Biol. 2010;12(6):533-42. Epub
760 20100509. doi: 10.1038/ncb2055. PubMed PMID: 20453849.
761 54. Sakakibara S, Mizutani K, Sugiura A, Sakane A, Sasaki T, Yonemura S, et al. Afadin
762 regulates actomyosin organization through alphaE-catenin at adherens junctions. J Cell Biol.
763 2020;219(5). doi: 10.1083/jcb.201907079. PubMed PMID: 32227204; PubMed Central PMCID:
764 PMCPMC7199863.
765 55. Maiden SL, Hardin J. The secret life of alpha-catenin: moonlighting in morphogenesis. J
766 Cell Biol. 2011;195(4):543-52. doi: 10.1083/jcb.201103106. PubMed PMID: 22084304;
767 PubMed Central PMCID: PMCPMC3257527.
768 56. Pettitt J, Cox EA, Broadbent ID, Flett A, Hardin J. The Caenorhabditis elegans p120
769 catenin homologue, JAC-1, modulates cadherin-catenin function during epidermal
770 morphogenesis. J Cell Biol. 2003;162(1):15-22. doi: 10.1083/jcb.200212136. PubMed PMID:
771 12847081; PubMed Central PMCID: PMCPMC2172718.
772 57. Lynch AM, Grana T, Cox-Paulson E, Couthier A, Cameron M, Chin-Sang I, et al. A
773 genome-wide functional screen shows MAGI-1 is an L1CAM-dependent stabilizer of apical
774 junctions in C. elegans. Curr Biol. 2012;22(20):1891-9. Epub 20120913. doi:
775 10.1016/j.cub.2012.08.024. PubMed PMID: 22981773; PubMed Central PMCID:
776 PMCPMC3482306.
777 58. Xu XP, Pokutta S, Torres M, Swift MF, Hanein D, Volkmann N, et al. Structural basis of
778 alphaE-catenin-F-actin catch bond behavior. Elife. 2020;9. Epub 20200911. doi:
779 10.7554/eLife.60878. PubMed PMID: 32915141; PubMed Central PMCID: PMCPMC7588230.
780 59. Li J, Newhall J, Ishiyama N, Gottardi C, Ikura M, Leckband DE, et al. Structural
781 Determinants of the Mechanical Stability of alpha-Catenin. J Biol Chem. 2015;290(31):18890-
782 903. Epub 20150612. doi: 10.1074/jbc.M115.647941. PubMed PMID: 26070562; PubMed
783 Central PMCID: PMCPMC4521009.
784 60. Terekhova K, Pokutta S, Kee YS, Li J, Tajkhorshid E, Fuller G, et al. Binding partner-
785 and force-promoted changes in alphaE-catenin conformation probed by native cysteine labeling.
786 Sci Rep. 2019;9(1):15375. Epub 20191025. doi: 10.1038/s41598-019-51816-3. PubMed PMID:
787 31653927; PubMed Central PMCID: PMCPMC6814714.
788 61. Barstead RJ, Waterston RH. The basal component of the nematode dense-body is
789 vinculin. Journal of Biological Chemistry. 1989;264(17):10177-85. doi: 10.1016/s0021-
790 9258(18)81782-3.
791 62. Lecroisey C, Brouilly N, Qadota H, Mariol MC, Rochette NC, Martin E, et al. ZYX-1,
792 the unique zyxin protein of Caenorhabditis elegans, is involved in dystrophin-dependent muscle
793 degeneration. Mol Biol Cell. 2013;24(8):1232-49. Epub 20130220. doi: 10.1091/mbc.E12-09-
794 0679. PubMed PMID: 23427270; PubMed Central PMCID: PMCPMC3623643.
795 63. Liu Q, Jones TI, Bachmann RA, Meghpara M, Rogowski L, Williams BD, et al. C.
796 elegans PAT-9 is a nuclear zinc finger protein critical for the assembly of muscle attachments.

797 Cell Biosci. 2012;2(1):18. Epub 20120522. doi: 10.1186/2045-3701-2-18. PubMed PMID:
798 22616817; PubMed Central PMCID: PMCPMC3419604.
799 64. Tachibana K, Nakanishi H, Mandai K, Ozaki K, Ikeda W, Yamamoto Y, et al. Two cell
800 adhesion molecules, nectin and cadherin, interact through their cytoplasmic domain-associated
801 proteins. J Cell Biol. 2000;150(5):1161-76. doi: 10.1083/jcb.150.5.1161. PubMed PMID:
802 10974003; PubMed Central PMCID: PMCPMC2175253.
803 65. Pokutta S, Drees F, Takai Y, Nelson WJ, Weis WI. Biochemical and structural definition
804 of the l-afadin- and actin-binding sites of alpha-catenin. J Biol Chem. 2002;277(21):18868-74.
805 Epub 20020320. doi: 10.1074/jbc.M201463200. PubMed PMID: 11907041; PubMed Central
806 PMCID: PMCPMC3368618.
807 66. Schmidt A, Lv Z, Grosshans J. ELMO and Sponge specify subapical restriction of Canoe
808 and formation of the subapical domain in early Drosophila embryos. Development. 2018;145(2).
809 Epub 20180126. doi: 10.1242/dev.157909. PubMed PMID: 29361564.
810 67. Manning LA, Perez-Vale KZ, Schaefer KN, Sewell MT, Peifer M. The Drosophila
811 Afadin and ZO-1 homologues Canoe and Polychaetoid act in parallel to maintain epithelial
812 integrity when challenged by adherens junction remodeling. Mol Biol Cell. 2019;30(16):1938-
813 60. Epub 20190612. doi: 10.1091/mbc.E19-04-0209. PubMed PMID: 31188739; PubMed
814 Central PMCID: PMCPMC6727765.
815 68. Walther RF, Burki M, Pinal N, Rogerson C, Pichaud F. Rap1, Canoe and Mbt cooperate
816 with Bazooka to promote zonula adherens assembly in the fly photoreceptor. J Cell Sci.
817 2018;131(6). Epub 20180326. doi: 10.1242/jcs.207779. PubMed PMID: 29507112; PubMed
818 Central PMCID: PMCPMC5897711.
819 69. Slovakova J, Speicher S, Sanchez-Soriano N, Prokop A, Carmena A. The actin-binding
820 protein Canoe/AF-6 forms a complex with Robo and is required for Slit-Robo signaling during
821 axon pathfinding at the CNS midline. J Neurosci. 2012;32(29):10035-44. doi:
822 10.1523/JNEUROSCI.6342-11.2012. PubMed PMID: 22815517; PubMed Central PMCID:
823 PMCPMC6621277.
824 70. Ma Z, Li P, Hu X, Song H. Polarity protein Canoe mediates overproliferation via
825 modulation of JNK, Ras-MAPK and Hippo signalling. Cell Prolif. 2019;52(1):e12529. Epub
826 20181017. doi: 10.1111/cpr.12529. PubMed PMID: 30328653; PubMed Central PMCID:
827 PMCPMC6430484.
828 71. Matsuo T, Takahashi K, Kondo S, Kaibuchi K, Yamamoto D. Regulation of cone cell
829 formation by Canoe and Ras in the developing Drosophila eye. Development.
830 1997;124(14):2671-80. doi: 10.1242/dev.124.14.2671. PubMed PMID: 9226438.
831 72. Callaci S, Morrison K, Shao X, Schuh AL, Wang Y, Yates JR, 3rd, et al.
832 Phosphoregulation of the C. elegans cadherin-catenin complex. Biochem J. 2015;472(3):339-52.
833 Epub 20151006. doi: 10.1042/BJ20150410. PubMed PMID: 26443865; PubMed Central
834 PMCID: PMCPMC4663164.
835 73. Raich WB, Agbunag C, Hardin J. Rapid epithelial-sheet sealing in the Caenorhabditis
836 elegans embryo requires cadherin-dependent filopodial priming. Curr Biol. 1999;9(20):1139-46.
837 doi: 10.1016/S0960-9822(00)80015-9. PubMed PMID: 10531027.
838 74. Mitchell SJ, Rosenblatt J. Early mechanical selection of cell extrusion and extrusion
839 signaling in cancer. Curr Opin Cell Biol. 2021;72:36-40. Epub 20210524. doi:
840 10.1016/j.ceb.2021.04.005. PubMed PMID: 34034216; PubMed Central PMCID:
841 PMCPMC8869604.

842 75. Tada M. The morphogenetic changes that lead to cell extrusion in development and cell
843 competition. Dev Biol. 2021;477:1-10. Epub 20210511. doi: 10.1016/j.ydbio.2021.05.003.
844 PubMed PMID: 33984304.
845 76. Villars A, Levayer R. Collective effects in epithelial cell death and cell extrusion. Curr
846 Opin Genet Dev. 2022;72:8-14. Epub 20211006. doi: 10.1016/j.gde.2021.09.004. PubMed
847 PMID: 34626896.
848 77. Harding MJ, McGraw HF, Nechiporuk A. The roles and regulation of multicellular
849 rosette structures during morphogenesis. Development. 2014;141(13):2549-58. doi:
850 10.1242/dev.101444. PubMed PMID: 24961796; PubMed Central PMCID: PMCPMC4067956.
851 78. Chuai M, Weijer CJ. The mechanisms underlying primitive streak formation in the chick
852 embryo. Curr Top Dev Biol. 2008;81:135-56. doi: 10.1016/S0070-2153(07)81004-0. PubMed
853 PMID: 18023726.
854 79. Rozbicki E, Chuai M, Karjalainen AI, Song F, Sang HM, Martin R, et al. Myosin-II-
855 mediated cell shape changes and cell intercalation contribute to primitive streak formation. Nat
856 Cell Biol. 2015;17(4):397-408. doi: 10.1038/ncb3138. PubMed PMID: 25812521; PubMed
857 Central PMCID: PMCPMC4886837.
858 80. Bertet C, Sulak L, Lecuit T. Myosin-dependent junction remodelling controls planar cell
859 intercalation and axis elongation. Nature. 2004;429(6992):667-71. doi: 10.1038/nature02590.
860 PubMed PMID: 15190355.
861 81. Blankenship JT, Backovic ST, Sanny JS, Weitz O, Zallen JA. Multicellular rosette
862 formation links planar cell polarity to tissue morphogenesis. Dev Cell. 2006;11(4):459-70. doi:
863 10.1016/j.devcel.2006.09.007. PubMed PMID: 17011486.
864 82. Saunders LR, McClay DR. Sub-circuits of a gene regulatory network control a
865 developmental epithelial-mesenchymal transition. Development. 2014;141(7):1503-13. Epub
866 20140305. doi: 10.1242/dev.101436. PubMed PMID: 24598159; PubMed Central PMCID:
867 PMCPMC3957374.
868 83. Miller JR, McClay DR. Changes in the pattern of adherens junction-associated beta-
869 catenin accompany morphogenesis in the sea urchin embryo. Dev Biol. 1997;192(2):310-22. doi:
870 10.1006/dbio.1997.8739. PubMed PMID: 9441670.
871 84. Simoes S, Oh Y, Wang MFZ, Fernandez-Gonzalez R, Tepass U. Myosin II promotes the
872 anisotropic loss of the apical domain during Drosophila neuroblast ingression. J Cell Biol.
873 2017;216(5):1387-404. Epub 20170331. doi: 10.1083/jcb.201608038. PubMed PMID:
874 28363972; PubMed Central PMCID: PMCPMC5412560.
875 85. Shao X, Lucas B, Strauch J, Hardin J. The adhesion modulation domain of
876 Caenorhabditis elegans alpha-catenin regulates actin binding during morphogenesis. Mol Biol
877 Cell. 2019;30(17):2115-23. Epub 20190612. doi: 10.1091/mbc.E19-01-0018. PubMed PMID:
878 31188702; PubMed Central PMCID: PMCPMC6743470.
879 86. Maiden SL, Harrison N, Keegan J, Cain B, Lynch AM, Pettitt J, et al. Specific conserved
880 C-terminal amino acids of Caenorhabditis elegans HMP-1/alpha-catenin modulate F-actin
881 binding independently of vinculin. J Biol Chem. 2013;288(8):5694-706. Epub 20121227. doi:
882 10.1074/jbc.M112.438093. PubMed PMID: 23271732; PubMed Central PMCID:
883 PMCPMC3581367.
884 87. Choi W, Acharya BR, Peyret G, Fardin MA, Mege RM, Ladoux B, et al. Remodeling the
885 zonula adherens in response to tension and the role of afadin in this response. J Cell Biol.
886 2016;213(2):243-60. doi: 10.1083/jcb.201506115. PubMed PMID: 27114502; PubMed Central
887 PMCID: PMCPMC5084271.

88. Sawyer JK, Choi W, Jung KC, He L, Harris NJ, Peifer M. A contractile actomyosin network linked to adherens junctions by Canoe/afadin helps drive convergent extension. Mol Biol Cell. 2011;22(14):2491-508. Epub 20110525. doi: 10.1091/mbc.E11-05-0411. PubMed PMID: 21613546; PubMed Central PMCID: PMCPMC3135475.
89. Sawyer JK, Harris NJ, Slep KC, Gaul U, Peifer M. The Drosophila afadin homologue Canoe regulates linkage of the actin cytoskeleton to adherens junctions during apical constriction. J Cell Biol. 2009;186(1):57-73. doi: 10.1083/jcb.200904001. PubMed PMID: 19596848; PubMed Central PMCID: PMCPMC2712996.
90. Yu HH, Zallen JA. Abl and Canoe/Afadin mediate mechanotransduction at tricellular junctions. Science. 2020;370(6520). doi: 10.1126/science.aba5528. PubMed PMID: 33243859; PubMed Central PMCID: PMCPMC8559527.
91. Edelstein A, Amodaj N, Hoover K, Vale R, Stuurman N. Computer control of microscopes using microManager. Curr Protoc Mol Biol. 2010;Chapter 14:Unit14 20. Epub 2010/10/05. doi: 10.1002/0471142727.mb1420s92. PubMed PMID: 20890901; PubMed Central PMCID: PMCPMC3065365.
92. Edelstein AD, Tsuchida MA, Amodaj N, Pinkard H, Vale RD, Stuurman N. Advanced methods of microscope control using μManager software. Journal of Biological Methods. 2014;1(2):10. doi: 10.14440/jbm.2014.36.
93. Dickinson DJ, Goldstein B. CRISPR-based methods for Caenorhabditis elegans genome engineering. Genetics. 2016;202(3):885-901. doi: 10.1534/genetics.115.182162. PubMed PMID: 26953268; PubMed Central PMCID: PMCPMC4788126.
94. Schwartz ML, Jorgensen EM. SapTrap, a Toolkit for High-Throughput CRISPR/Cas9 Gene Modification in Caenorhabditis elegans. Genetics. 2016;202(4):1277-88. Epub 2016/02/04. doi: 10.1534/genetics.115.184275. PubMed PMID: 26837755; PubMed Central PMCID: PMCPMC4905529.
95. Arribere JA, Bell RT, Fu BX, Artiles KL, Hartman PS, Fire AZ. Efficient marker-free recovery of custom genetic modifications with CRISPR/Cas9 in Caenorhabditis elegans. Genetics. 2014;198(3):837-46. Epub 2014/08/28. doi: 10.1534/genetics.114.169730. PubMed PMID: 25161212; PubMed Central PMCID: PMCPMC4224173.
96. Kamath RS, Ahringer J. Genome-wide RNAi screening in Caenorhabditis elegans. Methods. 2003;30(4):313-21. doi: 10.1016/s1046-2023(03)00050-1. PubMed PMID: 12828945.

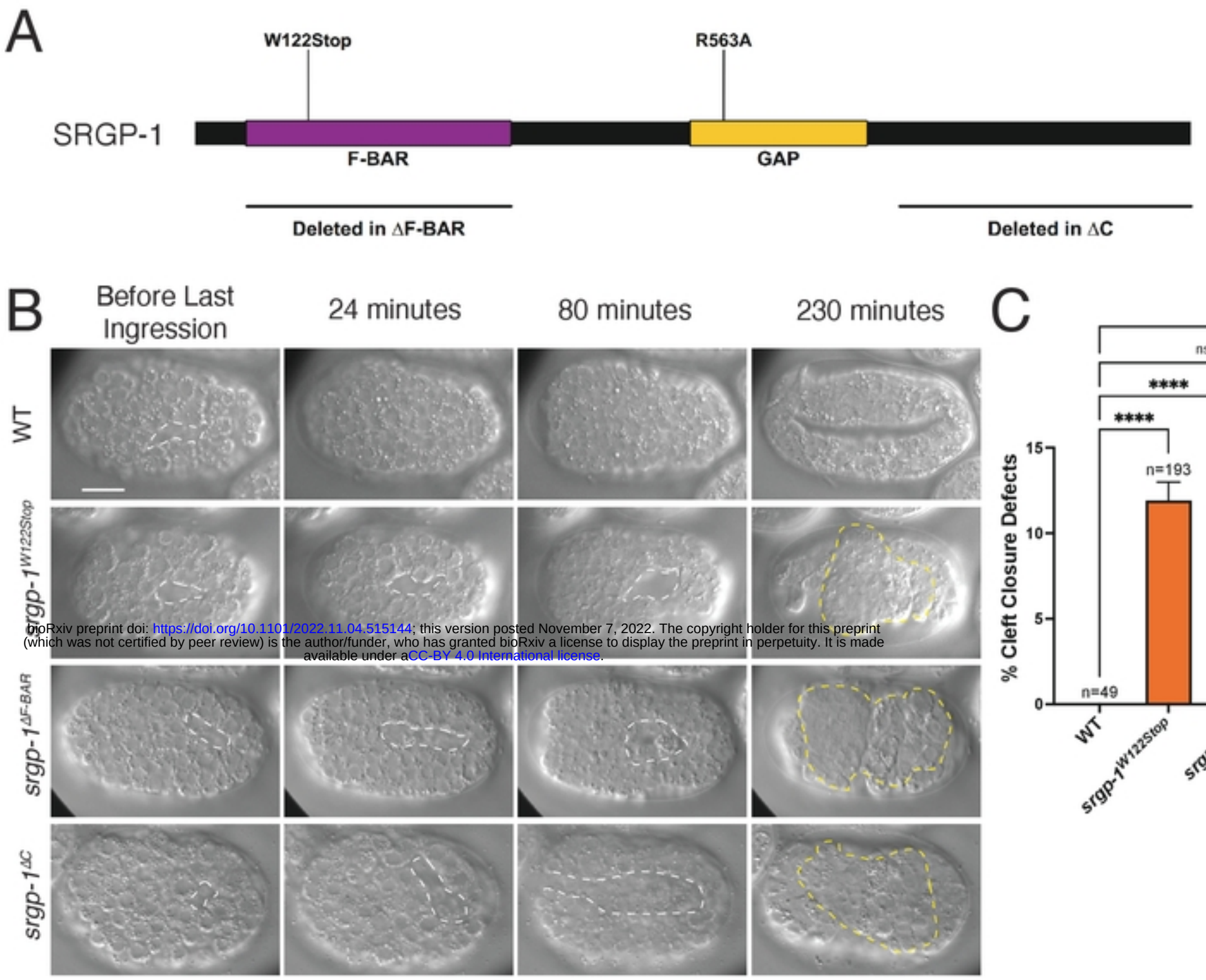

Figure 1

Figure 1

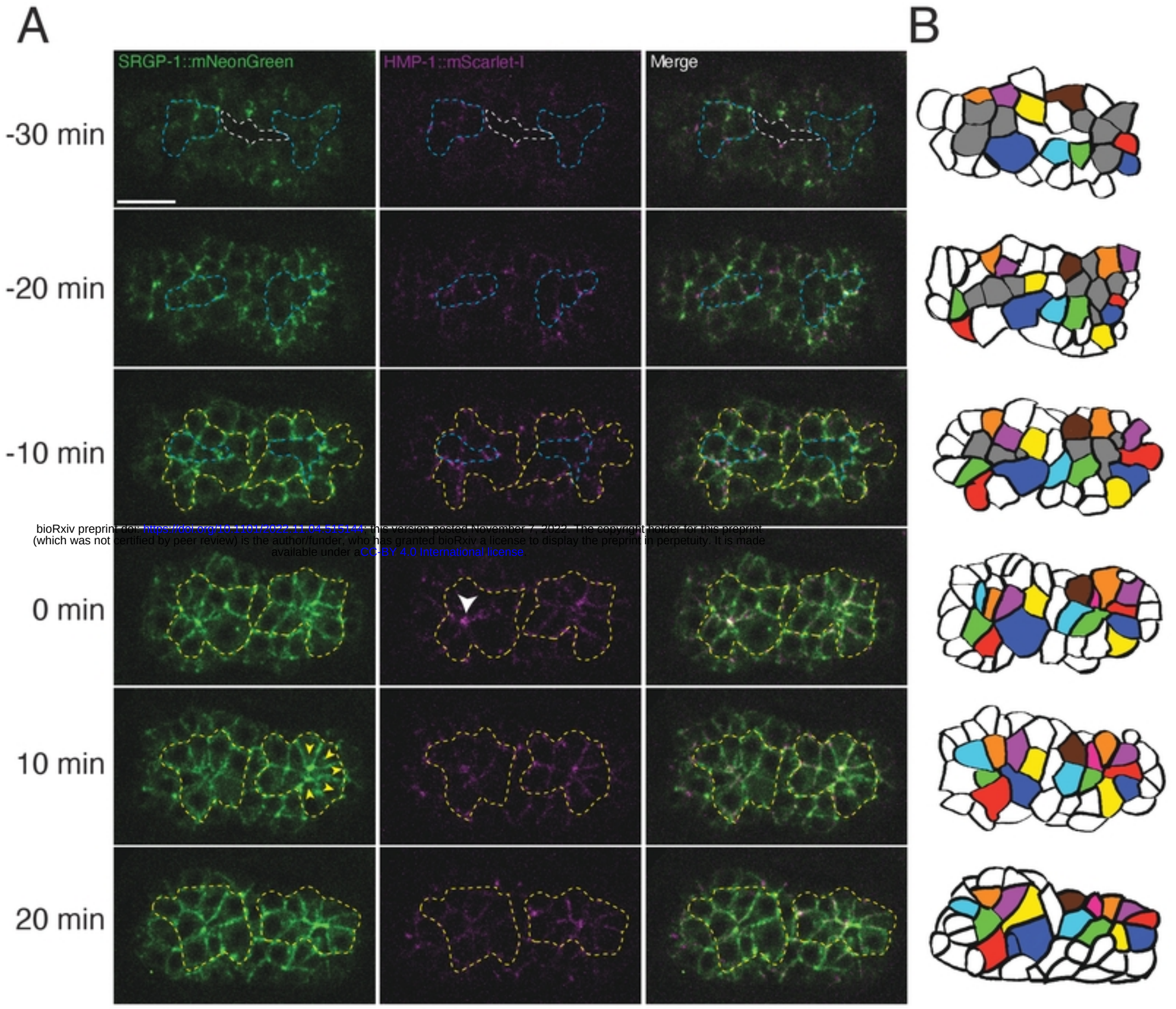

Figure 2

Figure 2

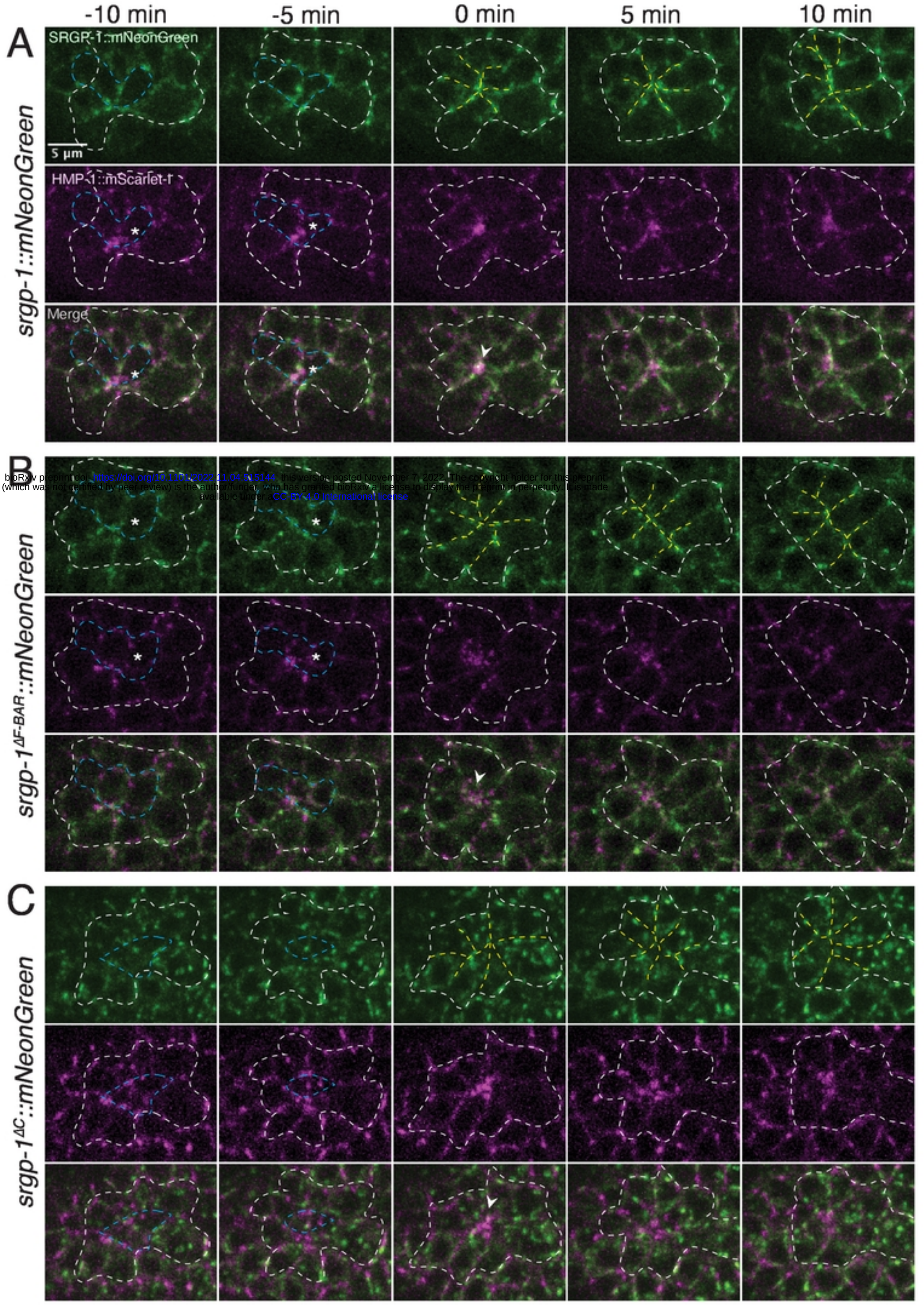

Figure 3

Figure 3

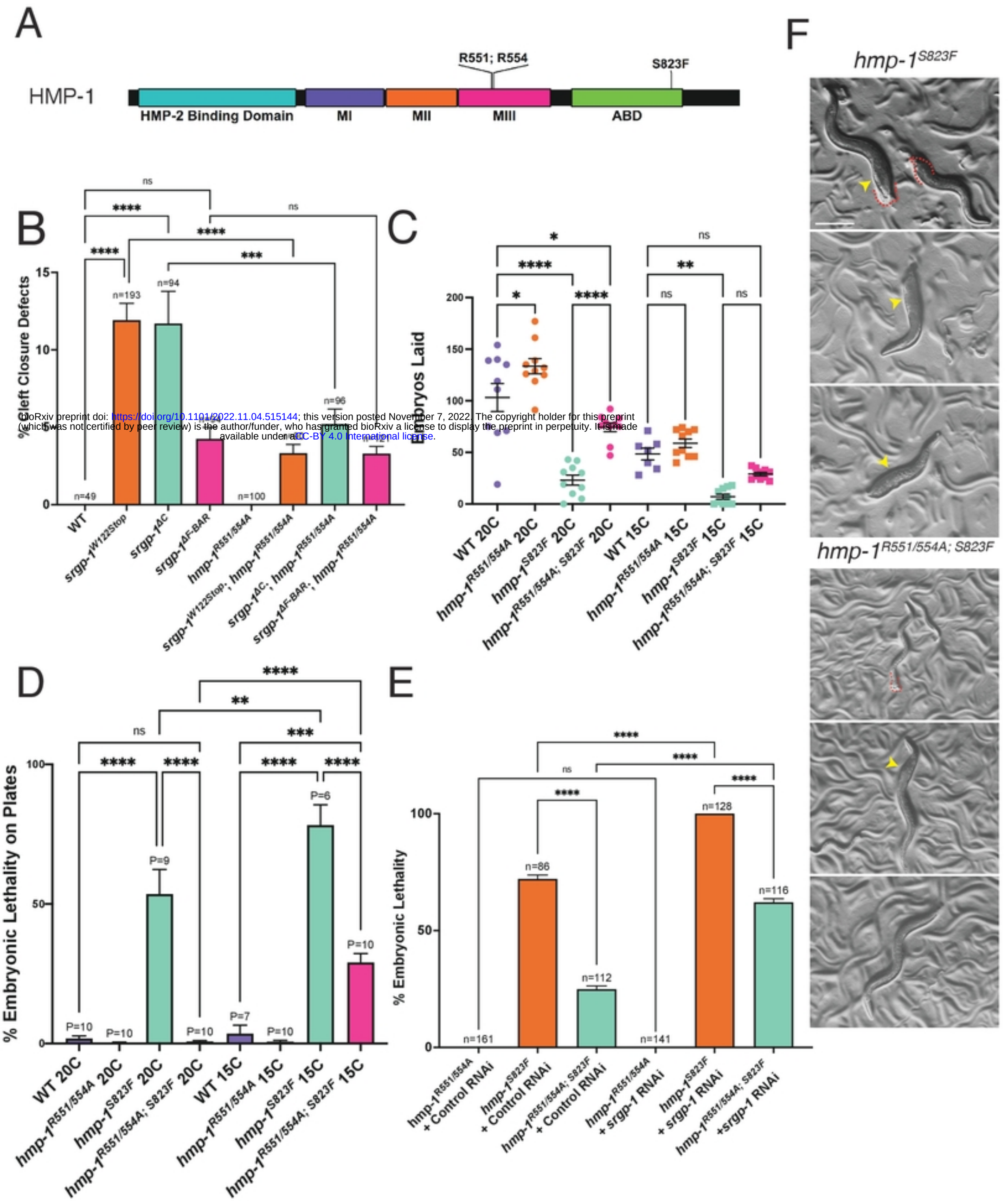

Figure 4

Figure 4

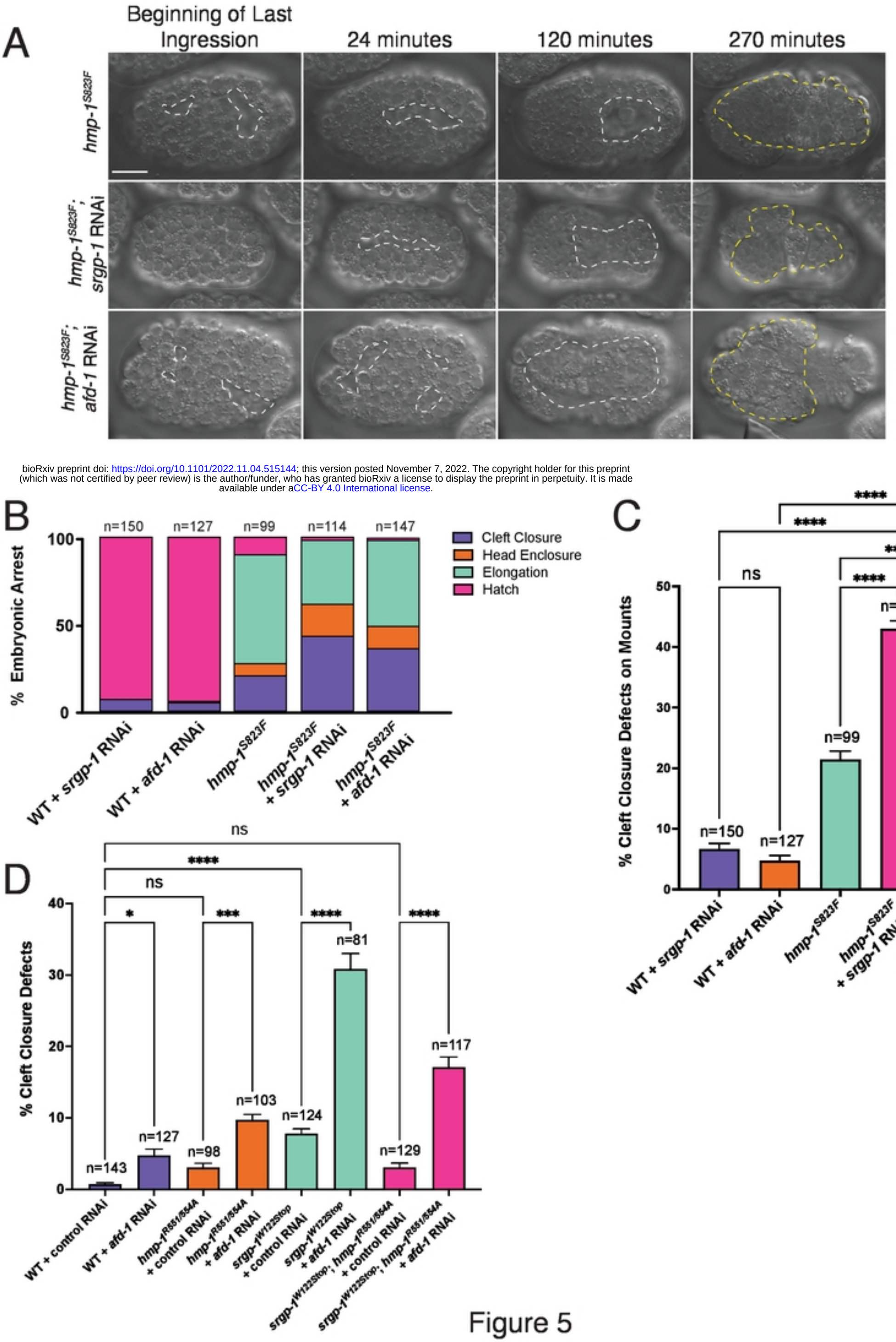

Figure 5

Figure 5

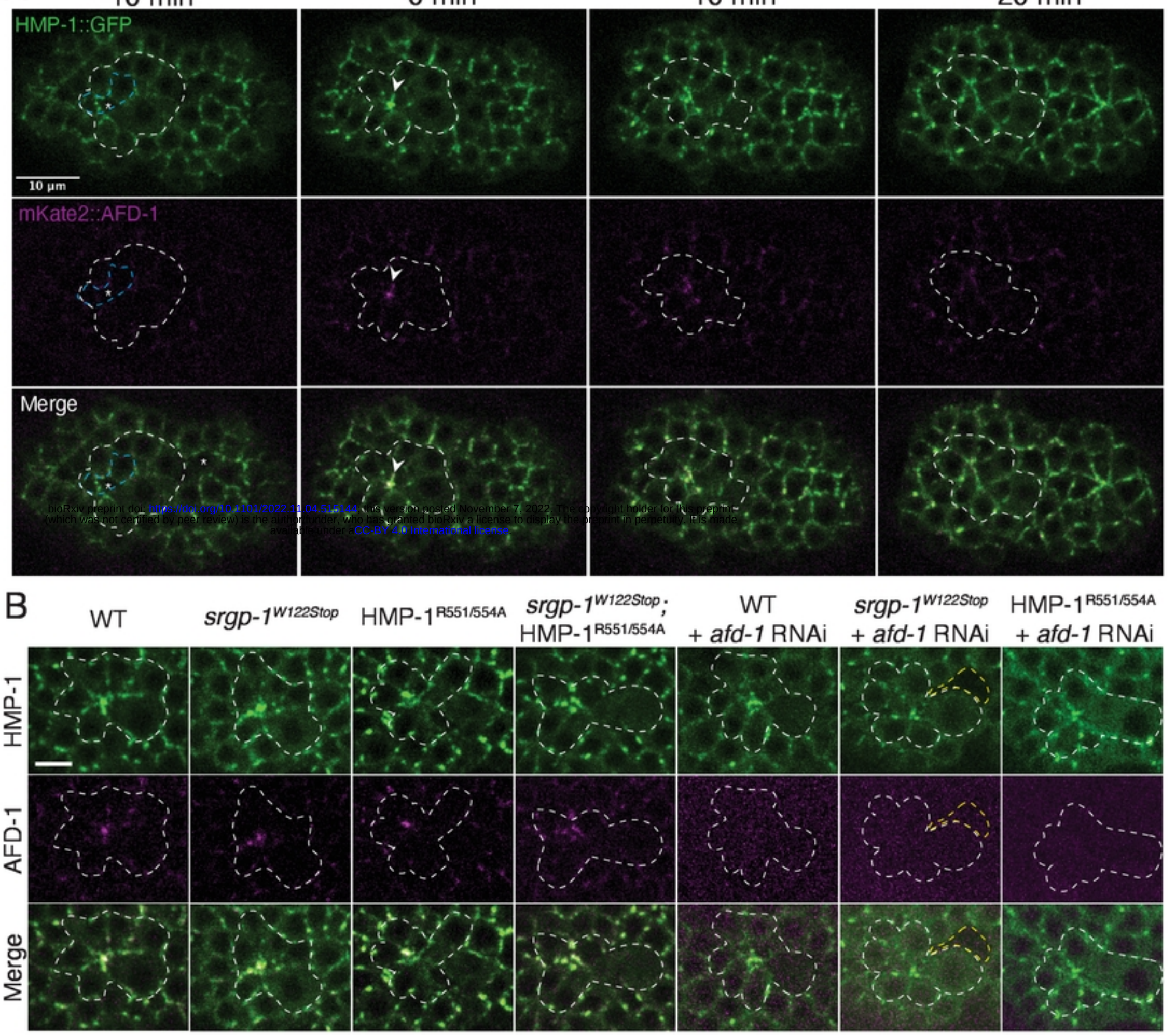

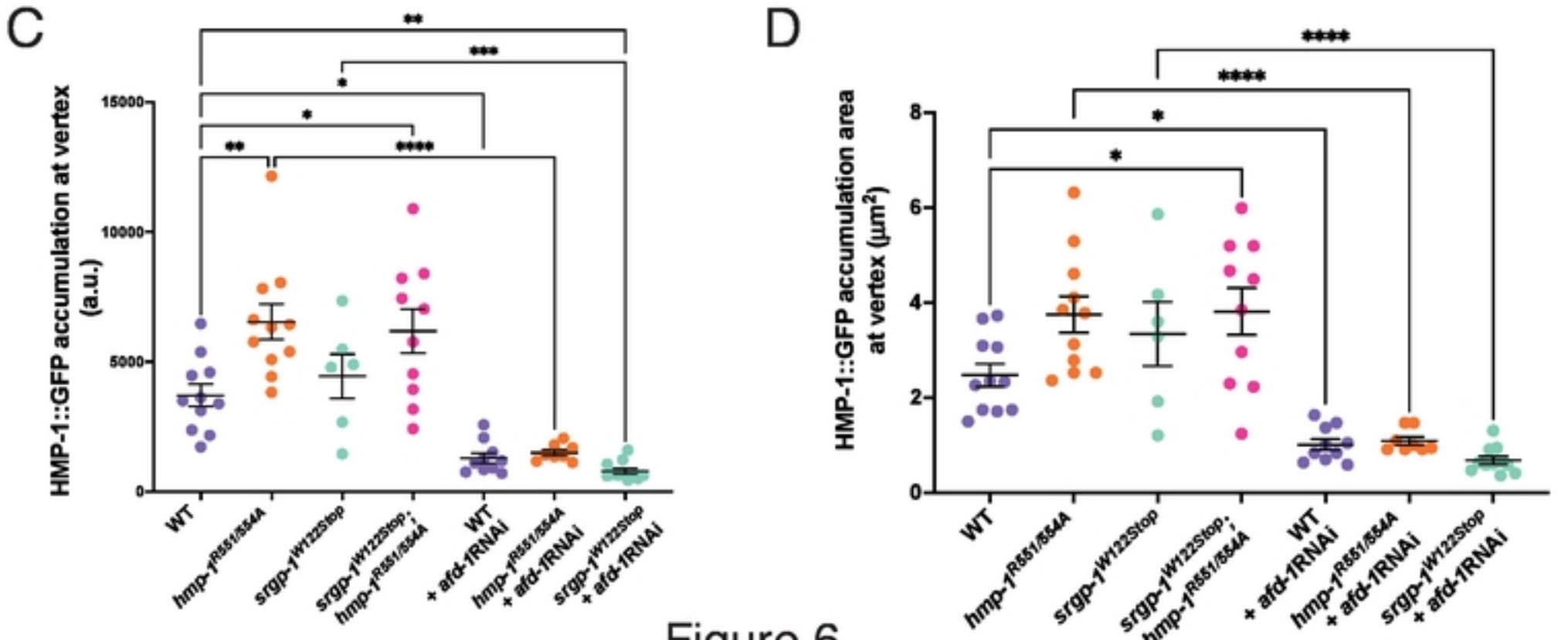

Figure 6

Figure 6

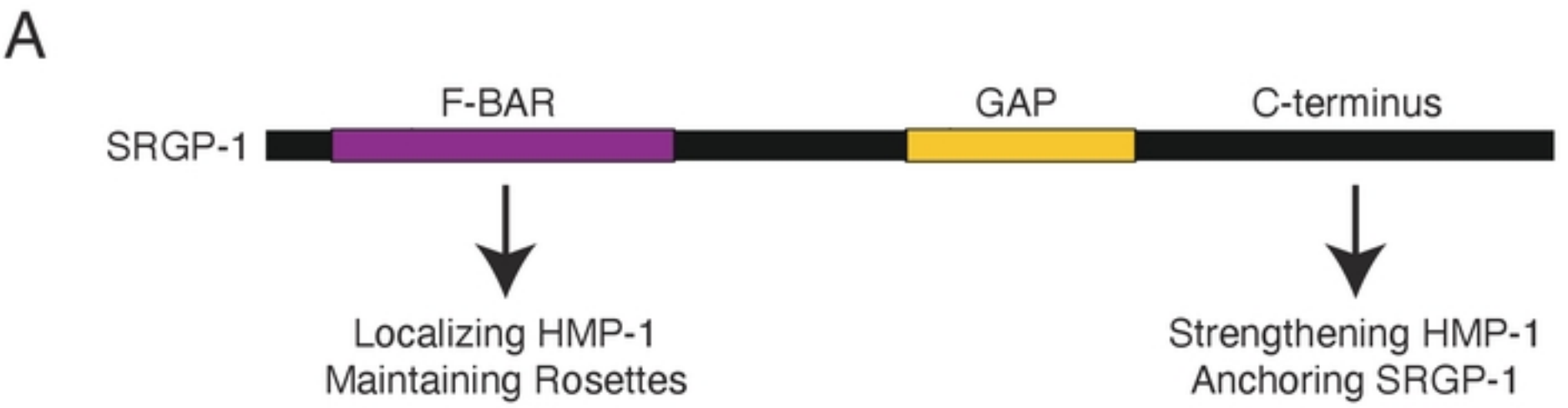

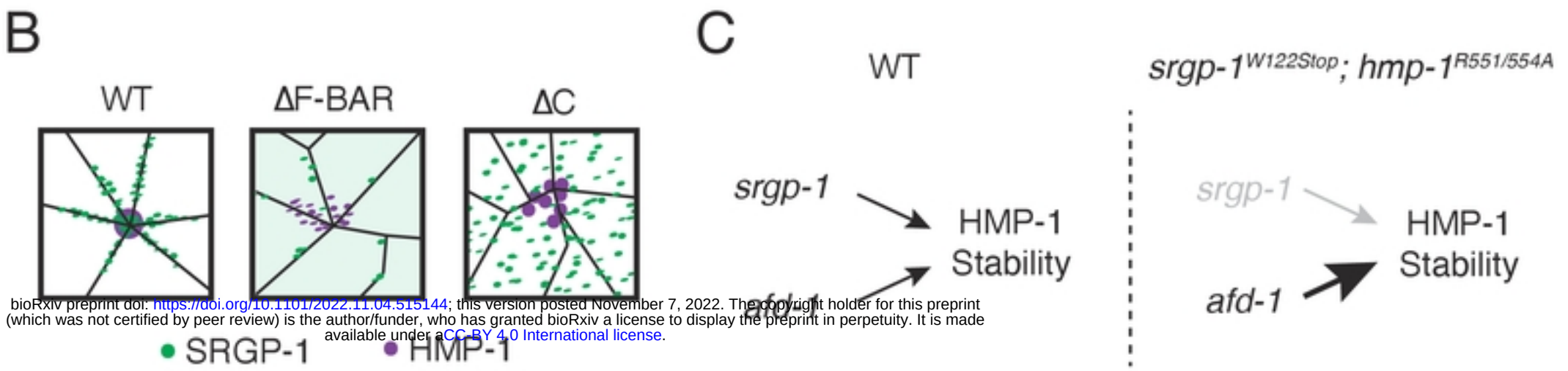

Figure 7

Figure 7